Molecular Plant Pathology

MOLECULAR PLANT PATHOLOGY (2012) **13**(5), 467–482 DOI: 10.1111/J.1364-3703.2011.00763.X

A functional genomics approach to dissect the mode of action of the *Stagonospora nodorum* effector protein SnToxA in wheat

DELPHINE VINCENT[1,†], LAUREN A. DU FALL[1,†], ANDREJA LIVK[2], ULRIKE MATHESIUS[1], RICHARD J. LIPSCOMBE[2], RICHARD P. OLIVER[3], TIMOTHY L. FRIESEN[4] AND PETER S. SOLOMON[1,*]

[1]*Research School of Biology, College of Medicine, Biology and Environment, The Australian National University, ACT 0200, Australia*
[2]*Proteomics International, Perth, WA 6000, Australia*
[3]*Curtin University of Technology, Perth, WA 6845, Australia*
[4]*USDA-ARS, Red River Valley Agricultural Research Center, Northern Crop Science Laboratory, Cereal Crops Research Unit, Fargo, ND 58102-2765, USA*

SUMMARY

In this study, proteomics and metabolomics were used to study the wheat response to exposure to the SnToxA effector protein secreted by the fungal pathogen *Stagonospora nodorum* during infection. Ninety-one different acidic and basic proteins and 101 metabolites were differentially abundant when comparing SnToxA- and control-treated wheat leaves during a 72-h time course. Proteins involved in photosynthesis were observed to increase marginally initially after exposure, before decreasing rapidly and significantly. Proteins and metabolites associated with the detoxification of reactive oxygen species in the chloroplast were also differentially abundant during SnToxA exposure, implying that the disruption of photosynthesis causes the rapid accumulation of chloroplastic reactive oxygen species. Metabolite profiling revealed major metabolic perturbations in central carbon metabolism, evidenced by significant increases in tricarboxylic acid (TCA) cycle intermediates, suggestive of an attempt by the plant to generate ATP and reducing equivalents in response to the collapse of photosynthesis caused by SnToxA. This was supported by the observation that the TCA cycle enzyme malate dehydrogenase was up-regulated in response to SnToxA. The infiltration of SnToxA also resulted in a significant increase in abundance of many pathogenicity-related proteins, even in the absence of the pathogen or other pathogen-associated molecular patterns. This approach highlights the complementary nature of proteomics and metabolomics in studying effector–host interactions, and provides further support for the hypothesis that necrotrophic pathogens, such as *S. nodorum*, appear to exploit existing host cell death mechanisms to promote pathogen growth and cause disease.

INTRODUCTION

Our understanding of fungal plant diseases has long been dominated by the concept of gene-for-gene interactions, first proposed by Flor in 1942 (Flor, 1942, 1956). This model has been well established for biotrophic pathogens, but, until recently, there has been little evidence that it holds true for the necrotrophic pathogens that feed off dying or dead tissue. The necrotrophs have long been viewed as simplistic pathogens that rely on a battery of lytic and degradative enzymes to obtain the required nutrients. Recent studies have overturned this simplistic model and have shown that many necrotrophs interact with the host in an elegantly specific gene-for-gene manner, albeit inversely (Friesen *et al*., 2008; Oliver and Solomon, 2010; Strelkov and Lamari, 2003). In such a system, the pathogen secretes small proteins, termed effectors, which are typically translocated into host cells. These effectors then appear to interact with a dominant susceptibility locus in a gene-for-gene manner, resulting in cell death. Rather than restricting cell growth as in a biotrophic interaction, cell death results in a rich nutrient source which promotes necrotrophic infection. The details of this interaction remain poorly understood, although it has been suggested that necrotrophs may exploit existing host death mechanisms that are usually associated with a resistant hypersensitive response (HR) (Hammond-Kosack and Rudd, 2008). This is known as effector-triggered susceptibility (ETS) based on the apparent manipulation by necrotrophs of the effector-triggered immunity defence mechanism.

The first proteinaceous necrotrophic effector identified was Ptr ToxA from *Pyrenophora tritici-repentis*, the causal agent of yellow (or tan) spot in wheat (*Triticum aestivum*) (Ballance *et al*., 1989; Tomas *et al*., 1990). The virulence of the fungus on wheat genotypes carrying the dominant susceptibility gene *Tsn1* is dependent on the production of the Ptr ToxA effector. Sensitivity to the purified effector protein co-locates to the same genetic locus as susceptibility to the disease (Faris *et al*., 1996; Tomas *et al*., 1990). *Tsn1* has now been cloned and possesses many of the features typically associated with resistance (*R*) genes, including serine/threonine protein kinase (S/TPK), nucleotide-binding site (NBS) and leucine-rich repeat (LRR) domains, all of which are required for Ptr ToxA sensitivity (Faris *et al*., 2010). Genome sequence analysis of the related wheat pathogen *Stagonospora nodorum* reveals that it harbours a homologue of *Ptr ToxA*, named *SnToxA* (Friesen *et al*., 2006). *SnToxA* is 99.7% identical to *Ptr ToxA*, which

**Correspondence*: Email: peter.solomon@anu.edu.au
†These authors contributed equally to this study.

is hypothesized to have been recently acquired by *P. triticirepentis* through a lateral gene transfer event (Friesen *et al*., 2006). Like Ptr ToxA, SnToxA only initiates leaf chlorosis and subsequent necrosis in the presence of *Tsn1* (Friesen *et al*., 2006).

Ciuffetti and co-workers (Manning and Ciuffetti, 2005; Manning *et al*., 2008) have provided evidence that Ptr ToxA, like many other fungal effectors (Kale *et al*., 2010), is likely to be translocated into host cells during growth of the pathogen *in planta*. It is unclear how Ptr ToxA is internalized, but the requirement for the solvent-exposed RGD domain has been demonstrated, as has the presence of *Tsn1* (Manning *et al*., 2008; Sarma *et al*., 2005). Protein binding studies have also shown that Ptr ToxA and Tsn1 do not interact directly, suggesting that Tsn1 is not a high-affinity receptor for ToxA (Faris *et al*., 2010). Once internalized, Ptr ToxA is targeted to the chloroplast, where it has been shown to bind to plastocyanin and ToxA binding protein 1 (ToxABP1). The function of ToxABP1 is unknown, but silencing in sensitive wheat lines results in reduced Ptr ToxA sensitivity (Manning *et al*., 2010; Tai *et al*., 2007). The localization of Ptr ToxA to the chloroplast is then followed by an accumulation of reactive oxygen species (ROS) in the presence of light and, ultimately, cell death (Manning and Ciuffetti, 2005; Manning *et al*., 2009).

These studies have provided significant insight into the mechanism and mode of action of Ptr ToxA. Two recent reports have sought to understand the host response to Ptr ToxA exposure using microarrays (Adhikari *et al*., 2009; Pandelova *et al*., 2009). Numerous cellular processes were highlighted as being up- and down-regulated in response to Ptr ToxA exposure, including photosynthesis, defence responses and pathways involved in the generation of ROS. Although the sequence similarity between Ptr ToxA and SnToxA is clear, there have been no mechanistic studies to date examining the mode of action of SnToxA, or the response of the host to SnToxA exposure. In this study, we have examined the host proteome and metabolome in response to SnToxA exposure. A proteomics approach was chosen because it has been well documented that the correlation between mRNA and protein levels is such that protein levels cannot always be predicted from quantitative mRNA data (Gygi *et al*., 1999). Metabolomics is a complementary technique to proteomics, but does, in itself, offer distinct advantages, namely that it is the metabolome rather than either the transcriptome or proteome that more directly influences the phenotype (Kell *et al*., 2005). The goals of this study were two-fold. First, we sought to determine the response at the level of the proteome and metabolome of a susceptible wheat variety to exposure to SnToxA. Second, we used the data generated to compare the modes of action of SnToxA and Ptr ToxA. The application of these complementary functional genomics techniques has identified that SnToxA and Ptr ToxA have comparable modes of action. This study also identified novel aspects of the response of wheat to SnToxA exposure and shed new light onto this necrotrophic gene-for-gene interaction.

RESULTS

SnToxA infiltration causes chlorosis of susceptible wheat leaves

Leaves from the *S. nodorum*-susceptible wheat genotype BG261 were infiltrated with either an SnToxA solution to initiate a reaction or water as a control, and sampled at 0.5, 4, 12, 24, 48 and 72 h post-infiltration (hpi). The infiltrated areas of control leaves remained undamaged over time (Fig. 1A). Symptoms became visible at 24 hpi in the SnToxA-infiltrated leaves and chlorosis developed gradually afterwards (Fig. 1B). Using the quantitative

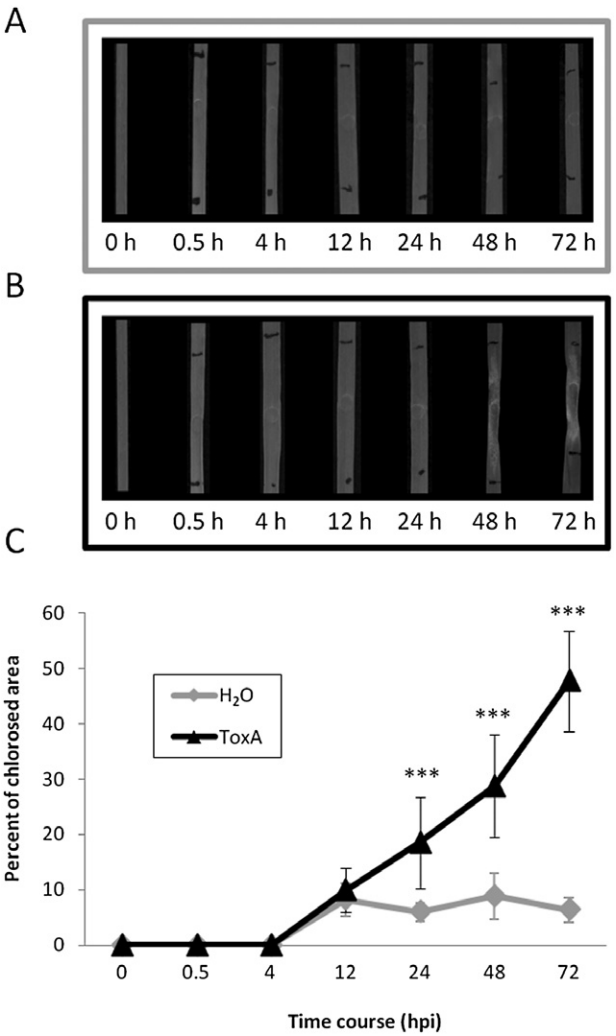

Fig. 1 Toxicity assay over 0–72 h post-infiltration (hpi) following wheat leaf infiltration with mock (H_2O) solution ($n = 5$) (A) and 1.22 μg/mL ToxA solution ($n = 10$) (B). (C) Chlorotic area within the infiltrated region (marked with horizontal black lines) was quantified using Scion Image software and converted into a percentage. Significance levels (***$P < 0.001$) were obtained using independent one-way analyses of variance (ANOVAs) for each time point.

method devised by Wijekoon *et al*. (2008), the chlorotic surface area was measured (Fig. 1C). Damage caused by infiltration *per se* was assessed in water-infiltrated leaves. Symptoms of minor physical damage were apparent at 12 hpi and were stable over time, affecting approximately 10% of the infiltrated area. Consistent with this damage, SnToxA treatment also affected 10% of the infiltrated area at 12 hpi. The percentage of chlorosis increased steadily in SnToxA-infiltrated leaves, and reached approximately 20% at 24 hpi, 30% at 48 hpi and 50% at 72 hpi. Complete necrosis of the infiltrated region was apparent by 7 days post-infiltration (data not shown).

A proteomics approach to resolve the wheat response to ToxA exposure

A gel-based proteomics strategy was adopted in this study using two-dimensional electrophoresis to separate wheat leaf acidic and basic soluble proteins, in combination with tandem mass spectrometry (MS/MS) for identification. Overall, two-dimensional patterns were of acceptable quality, with few streaks, especially for basic proteins, and well-resolved spots covering the whole gel (Fig. 2). Along the acidic gradient, the 55-kDa horizontal streak and the two most prominent 15-kDa spots represent ribulose bisphosphate carboxylase/oxygenase (RuBisCO) large and small subunits (RBCL and RBCS; spots A229, A290, A839–842, B066, B084, B216), respectively. RuBisCO has been shown previously to represent more than 50% of the soluble proteins in wheat photosynthetic tissue (Parry *et al*., 2011). In our study, although the large subunit of RuBisCO is too prominent to be resolved along a range of pH 4–7, it does not affect the rest of the two-dimensional pattern. Table S1 (see Supporting Information) lists the experimental features and reports the number of protein spots separated along acidic and basic ranges. Although the protein content loaded onto basic immobilized pH gradient (IPG) strips was five times higher than that on acidic strips, it only yielded half the number of spots (1070 acidic spots versus 530 basic spots). However, the incorporation of basic proteins in this study increased protein coverage by 50%.

Approximately one-half of the detected spots were deemed to be reproducible when present in two of three biological replicates (520 acidic spots and 218 basic spots), and their expression profiling was explored using analyses of variance (ANOVAs). Two-way ANOVAs showed that 213 (41%) acidic spots and 167 (77%) basic spots were significantly [$P < 0.1$, false discovery rate (FDR) correction] affected under our experimental conditions, amounting to 380 (51%) spots in total (Table S2, see Supporting Information). Of these, 260 (68%) spots responded to the time (TI) factor, 52 (14%) spots responded to the treatment (TR) factor and 68 (18%) spots responded to the TI × TR interaction effect. Overall, more basic proteins than acidic proteins were significant in our design and, in particular, 78 (47%) of the basic proteins responded to TR and/or TI × TR effects, whereas only 42 (20%) of the acidic proteins presented the same pattern. All the proteins with TR and/or TI × TR effects were selected for protein identification, and some spots whose abundance varied significantly over time were also included.

A total of 76 acidic spots and 54 basic spots underwent matrix-assisted laser desorption ionization time-of-flight tandem mass spectrometry (MALDI TOF/TOF MS/MS) analyses (Fig. 2). Of the 130 MS-analysed spots, 110 (85%) led to successful protein identifications (including proteins of unknown function). Most of the annotations came from cereals (79%), and *Triticum* species in particular (57%). Complementing MALDI-TOF/TOF MS/MS analyses with nanoflow liquid chromatography electrospray ionization tandem mass spectrometry (nLC-ESI-MS/MS) analyses greatly improved the success rate of protein identification of both acidic and basic spots (92% and 74%, respectively). In some instances, two to three proteins were identified within the same spot (Table S3, see Supporting Information). The 110 hits obtained led to 91 different accessions, 81 of which were unique descriptions (Table 1). This highlights the high frequency of isoforms, with up to five identified forms (e.g. RuBisCO small subunit). Many of the acidic and basic proteins identified were suggestive that the exposure of susceptible wheat leaves to SnToxA caused significant changes in photosynthesis, oxidative stress and defence responses (Tables 1 and S3). These changes are discussed further in the following discussion.

Figure 3 displays the expression profiling of MS-analysed proteins in ToxA-infiltrated leaves relative to controls. Greater than 30% of the identified acidic proteins were significantly more abundant at 12 hpi. This trend was reversed at 48 hpi, with approximately the same number of proteins less abundant in treated leaves compared with the controls. Basic protein abundance was only measured in the 24- and 48-hpi samples, and showed that the number of proteins more or less abundant compared with the control increased at the latter time point.

Many of the identified SnToxA-responsive proteins are targeted to the chloroplast

The TargetP algorithm was used to determine the cell compartments to which the identified proteins were allocated (Table S3). Four proteins were predicted to be mitochondrial, 11 (mostly basic) to be secreted, 53 (34%) to be targeted to the chloroplast and 51 located elsewhere. The ChloroP algorithm was also used and predicted that 44% of the proteins were targeted to the chloroplast. Both algorithms operate solely on sequence information, searching for chloroplast transit peptide (cTP), mitochondrial targeting peptide (mTP) or secretory pathway signal peptide (SP). However, other proteins identified in this study, whether enzymes or structural proteins, are known to be chloroplastic and were missed by these predictions. This was the case for two isoforms of the RuBisCO large subunit (spots A229, A290, B127),

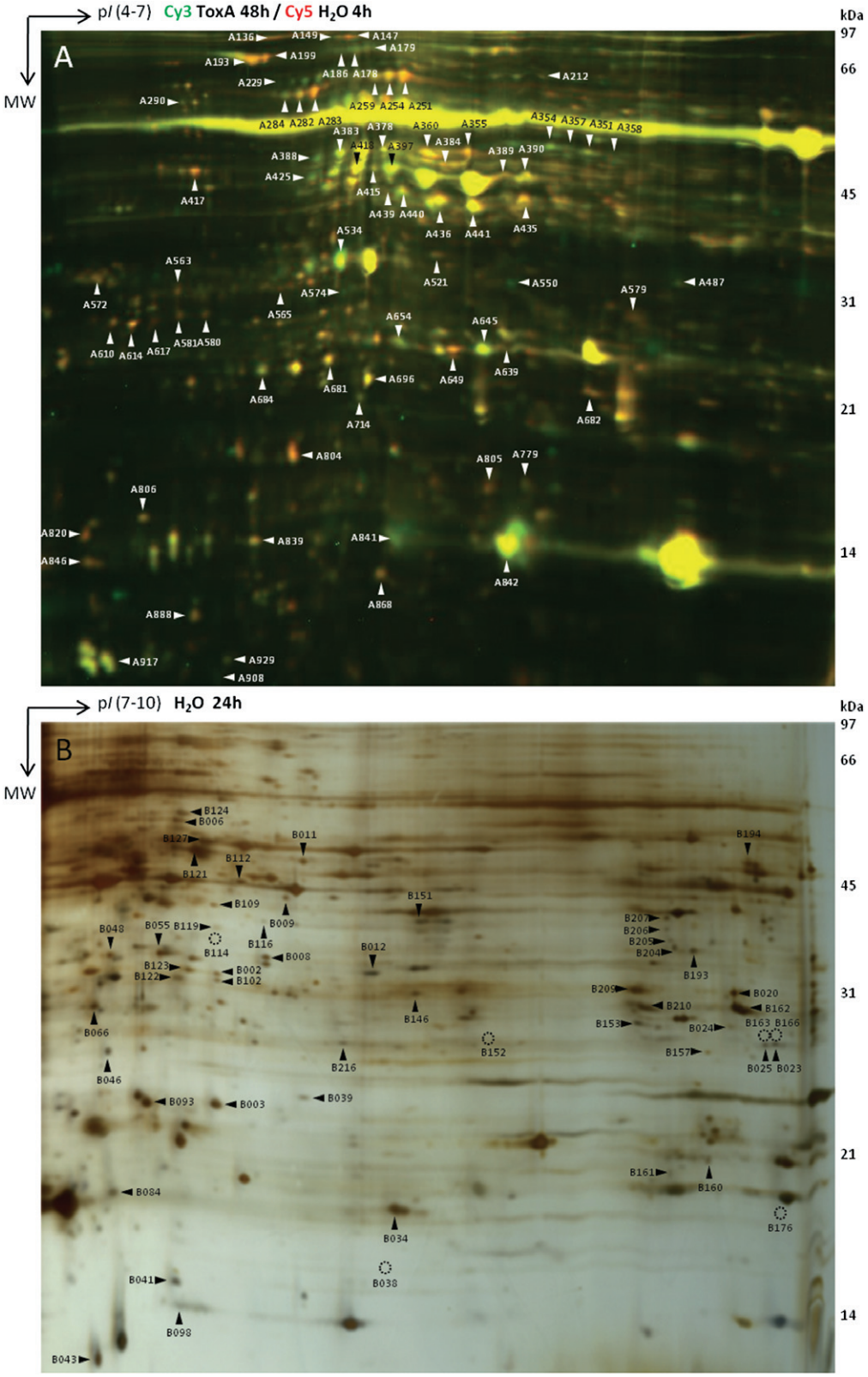

Fig. 2 Two-dimensional gels along acidic range (pH 4–7) following DIGE labelling (A) and basic range (pH 7–10) (B). Spots excised and analysed by mass spectrometry are indicated by an arrow when present or an open circle when missing.

Table 1 Identities of differentially expressed proteins in SnToxA-treated wheat.

Spot	Description	Accession	MASCOT score	Coverage (%)	log_2 ratio 0.5 h	log_2 ratio 4 h	log_2 ratio 12 h	log_2 ratio 24 h	log_2 ratio 48 h
A136	Heat shock protein (90 kDa)	Q43638	385	14	–0.906	0.852	0.953	–0.682	–0.489
A147	Putative uncharacterized protein Sb06g023840	C5YCZ2	664	16	–0.309	1.351	1.008	–1.014	–1.376
A149	Translation elongation factor G	C5YCZ2	719	18	0.056	2.053	1.288	–0.708	–1.439
A178	Heat shock cognate protein 70	Q6QUX5	361	16	0.347	–0.319	0.571	0.652	–0.249
A179	Heat shock cognate protein 70	Q6QUX5	370	15	0.527	–0.337	0.674	1.179	–0.942
A186	Heat shock protein 70	Q5MGA8	259	12	0.098	0.097	1.093	0.415	–0.854
A193	70-kDa heat shock protein	C7ENF7	632	14	–0.286	0.161	0.831	0.033	–0.607
A199	Heat shock protein 70	D2D320	95	7	–0.020	0.451	0.315	0.969	–1.176
A212	2,3-Bisphosphoglycerate-mutase	A8QPL0	163	25	0.188	–0.964	0.566	0.118	0.227
A229	Ribulose bisphosphate carboxylase/oxygenase (RuBisCO) large chain	B6GUT8	94	5	0.103	0.167	–0.915	1.006	1.331
A251	RuBisCO large subunit-binding protein subunit β	Q43831	335	15	0.600	0.266	0.371	0.098	–1.331
A254	RuBisCO large subunit-binding protein subunit β	Q43831	686	21	–0.436	0.213	0.466	–0.344	–0.044
A259	RuBisCO large subunit-binding protein subunit β	Q43831	679	20	0.089	0.466	0.500	0.237	–1.018
A282	RuBisCO large subunit-binding protein subunit α	P08823	1217	29	–0.292	0.405	0.418	0.145	–0.394
A283	RuBisCO large subunit-binding protein subunit α	P08823	1267	31	–0.347	0.359	0.752	0.316	–0.998
A284	RuBisCO large subunit-binding protein subunit α	P08823	975	29	–0.171	0.470	1.113	0.398	–1.265
A290	Ribulose bisphosphate carboxylase large chain (fragment)	Q6VW42	66	4	1.002	0.270	–0.645	–0.830	0.163
A351	*S*-Adenosylmethionine synthase 1	A6XMY9	808	39	0.654	0.449	0.108	0.351	0.594
A354	*S*-Adenosylmethionine synthase 3	Q4LB22	768	28	0.215	0.566	0.336	0.443	0.285
A355	Elongation factor Tu	C0P699	280	11	–0.520	–0.024	0.357	0.268	–0.388
A357	*S*-Adenosylmethionine synthase 3	Q4LB22	193	15	–0.313	0.147	0.998	0.050	1.136
A358	1-Deoxy-D-xylulose 5-phosphate reductoisomerase, putative	Q4H1G4	129	11	0.374	0.531	0.471	0.118	–0.094
A358	*S*-Adenosylmethionine synthase 1	Q70EZ8	153	6	0.374	0.531	0.471	0.118	–0.094
A360	RuBisCO activase A, chloroplastic	Q40073	620	20	0.017	0.051	0.761	–0.370	–0.606
A378	Plastid glutamine synthetase	C7DPL0	350	19	–0.275	0.307	0.914	–1.111	–0.106
A383	Plastid glutamine synthetase	C7DPL0	479	23	–0.431	0.319	0.470	–0.268	–0.418
A384	Phosphoglycerate kinase, chloroplastic	P12782	976	26	0.691	0.787	0.171	–1.239	–1.036
A388	Plastid glutamine synthetase	C7DPL0	284	16	–0.252	–0.031	0.217	–0.119	0.060
A389	RuBisCO activase A, chloroplastic	Q40073	624	22	1.365	1.390	–0.566	0.858	–1.817
A390	RuBisCO activase A, chloroplastic	Q40073	590	23	–0.066	0.196	0.471	–0.161	–0.936
A397	RuBisCO activase A, chloroplastic	Q40073	607	22	–0.520	0.100	0.539	–0.149	–0.338
A415	Sedoheptulose-1,7-bisphosphatase, chloroplastic	P46285	219	26	0.242	0.133	0.877	–0.857	–0.520
A417	Translation elongation factor G	A2XG06	277	16	–0.658	–0.508	–0.270	0.365	0.174
A418	Phosphoribulokinase, chloroplastic	P26302	739	34	–0.189	0.483	0.577	–0.511	–0.798
A425	Phosphoribulokinase, chloroplastic	P26302	249	15	–0.403	0.107	0.090	0.310	0.106
A435	Fructose-bisphosphate aldolase, chloroplastic	C0KTA6	392	16	0.027	0.089	0.721	–0.244	–0.772
A436	Fructose-bisphosphate aldolase, chloroplastic	C0KTA6	535	23	–0.011	0.211	0.710	–0.116	–0.987
A439	Fructose-bisphosphate aldolase, chloroplastic	C0KTA6	169	11	0.709	0.026	–1.736	–0.988	0.757
A440	Fructose-bisphosphate aldolase, chloroplastic	C0KTA6	459	21	–0.226	0.323	0.503	–0.457	–0.544
A441	Fructose-bisphosphate aldolase, cytosolic	B4FR47	283	8	–0.026	0.221	1.030	–0.195	–1.274
A487	Ribosomal protein L1	C5YXG6	166	8	–0.766	–0.596	0.482	–0.240	0.897
A521	Tyrosine phosphatase, putative	D5LXX6	103	19	0.091	0.435	0.383	–0.305	–0.756
A534	Chloroplast oxygen-evolving enhancer protein 1	A5JV93	396	30	–0.255	0.053	0.573	–0.259	0.034
A550	β-1,3-Glucanase	Q9XEN5	114	11	1.317	1.172	–0.411	–0.818	1.175
A563	14-3-3-like protein A	P29305	223	24	0.008	0.085	0.321	0.426	–0.520
A565	14-3-3 protein	Q08G36	344	29	–0.800	0.407	0.844	0.905	–1.249
A572	28-kDa ribonucleoprotein, chloroplast	O23798	421	30	–0.494	0.316	1.002	–0.231	–0.509
A574	Chloroplast lipocalin	Q38JB6	96	10	0.053	0.206	1.250	0.410	–1.731
A579	NAD-dependent epimerase/dehydratase	A2XZK1	109	9	–0.661	–0.246	0.745	0.501	–0.526
A580	Elongation factor 1-β	P29546	79	13	–0.159	0.671	0.777	–0.612	–0.684
A581	Elongation factor 1-β	P29546	108	11	0.577	0.394	0.403	0.309	–0.894
A610	29-kDa ribonucleoprotein, chloroplast	A2YNZ1	96	6	–0.059	0.315	0.629	0.297	–0.330
A614	Nucleic acid-binding protein, putative	C3V134	473	59	–0.240	0.104	0.365	–0.043	–0.043
A617	Nucleic acid-binding protein, putative	O81988	195	15	–0.339	0.245	0.246	–0.429	1.556
A639	Triosephosphate isomerase, cytosolic	P34937	247	17	–0.889	0.353	0.502	0.575	–0.887
A645	Oxygen-evolving enhancer protein 2, chloroplastic	Q00434	790	47	–0.668	0.037	0.392	0.284	–0.178
A649	Oxygen-evolving enhancer protein 2, chloroplastic	B8B3P0	188	11	–0.041	0.150	0.340	0.217	–0.946
A649	Chaperonin 21, putative	Q00434	76	6	–0.041	0.150	0.340	0.217	–0.946
A654	2-Cys peroxiredoxin BAS1, chloroplastic	A2YWS7	180	9	–0.389	0.194	0.930	0.509	–0.750
A654	Oxygen-evolving enhancer protein 2, chloroplastic	P80602	194	25	–0.389	0.194	0.930	0.509	–0.750
A654	Thylakoid lumenal 19-kDa protein	Q00434	166	27	–0.389	0.194	0.930	0.509	–0.750
A681	2-Cys peroxiredoxin BAS1, chloroplastic	P80602	670	44	–0.177	0.454	0.529	–0.040	–0.799
A682	50S ribosomal protein L10	B4G1Q5	131	8	–0.115	–0.306	0.553	–0.089	–0.287
A684	2-Cys peroxiredoxin BAS1, chloroplastic	P80602	486	53	–0.351	0.207	0.302	0.090	–0.343
A696	Chlorophyll *a*–*b*-binding protein 6A	C1K5B4	156	9	–0.206	0.344	0.687	–0.304	–1.047
A779	Nucleoside diphosphate kinase	Q0IMS5	162	17	1.065	–0.035	–0.470	–0.746	0.975
A804	50S ribosomal protein L12-1, chloroplastic	Q06030	91	14	0.029	0.083	0.154	–0.133	–0.314
A820	Histone H2B	B4FYZ0	73	16	0.147	0.257	0.544	–0.157	–0.281
A839	Ribulose bisphosphate carboxylase small chain	Q5NDA6	453	38	–0.103	0.124	0.440	–0.246	–0.782

Table 1 *Continued*.

Spot	Description	Accession	MASCOT score	Coverage (%)	log_2 ratio 0.5 h	log_2 ratio 4 h	log_2 ratio 12 h	log_2 ratio 24 h	log_2 ratio 48 h
A839	Thioredoxin M	Q9FRZ4	76	11	–0.103	0.124	0.440	–0.246	–0.782
A841	Ribulose bisphosphate carboxylase small chain	Q9FRZ4	146	16	–0.171	–0.009	0.440	0.219	0.079
A842	Ribulose bisphosphate carboxylase small chain	Q9FRZ4	193	22	–0.439	0.073	0.552	–0.077	–0.365
A846	60S acidic ribosomal protein P2-like protein	Q7X729	115	10	0.136	0.073	0.455	0.146	–0.487
A917	Plastocyanin, chloroplastic	P08248	101	20	–0.175	0.138	0.328	–0.244	–0.335
A929	Plastocyanin, chloroplastic	A2Z9R0	63	11	–0.087	–0.139	0.544	–0.105	–0.799
A929	Thylakoid membrane phosphoprotein 14 kDa, chloroplast	Q0DFC9	82	20	–0.087	–0.139	0.544	–0.105	–0.799
B003	Peptidyl-prolyl *cis–trans*-isomerase (cyclophilin)	Q6XPZ4	310	35				0.074	–0.158
B006	Geranylgeranyl hydrogenase	COLIR3	467	26				–0.204	–0.586
B006	UDP-sulphoquinovose synthase	D5GWI4	220	49				–0.204	–0.586
B006	Sulpholipid biosynthesis protein	Q45FE7	208	12				–0.204	–0.586
B008	Mg-protoporphyrin IX methyltransferase	Q5NKT1	98	6				–0.155	–0.518
B012	Adenylate kinase 1, putative	A9PB19	164	13				0.292	–0.039
B020	Mitochondrial outer membrane porin	P46274	287	21				0.429	–0.363
B023	Thaumatin-like protein	Q8S4P7	99	14				1.858	16.985
B024	Chitinase 1	Q8W429	175	21				2.101	17.392
B025	Transducin family protein	D7LEK9	50	1				0.000	16.975
B034	Ubiquitin carrier protein	C0PPR9	80	25				–0.007	0.777
B038	PR-4 (fragment)	Q9SQG3	82	10				0.000	16.656
B043	Ubiquitin monomer protein (fragment)	Q2VJ43	163	25				0.027	0.307
B046	Phenylalanine ammonia-lyase	D5KS97	224	6				–0.035	1.410
B048	Catalytic/coenzyme-binding protein	D7M797	84	9				0.006	–0.148
B055	Peroxisomal ascorbate peroxidase	A5JPR2	151	12				–0.013	–0.181
B055	Transcription factor APFI	Q8GRK1	171	18				–0.013	–0.181
B066	Carbonic anhydrase	D4N8D8	254	32				–0.220	–0.381
B066	Ribulose bisphosphate carboxylase small chain	Q9FRZ4	69	14				–0.220	–0.381
B084	Ribulose bisphosphate carboxylase small chain	Q9FRZ4	201	12				–0.504	–0.411
B093	Peptidyl-prolyl *cis–trans*-isomerase (cyclophilin)	Q6XPZ4	130	21				0.002	–0.237
B098	Photosystem II polypeptide 10 kDa (fragment)	Q6XW17	135	29				0.200	0.536
B109	5,10-Methylene-tetrahydrofolate dehydrogenase/5,10-methenyl-tetrahydrofolate cyclohydrolase	A6XMY4	213	17				0.036	–0.534
B112	RNA-binding protein, putative	Q9SA52	117	4				0.201	–0.535
B116	Chitinase	A5AT00	89	7				0.000	17.110
B119	31.7-kDa class I endochitinase-antifreeze protein	Q9AXR9	108	11				–0.198	1.914
B121	Hydroxypyruvate reductase	Q93XV7	106	9				0.286	–0.648
B122	Carbonic anhydrase	D4N8D8	179	25				–0.280	–1.536
B123	Plastidial outer membrane protein porin	A2WRY9	99	8				–0.062	–0.480
B127	Ribulose bisphosphate carboxylase large chain (fragment)	Q6QE22	46	4				–0.585	–0.376
B146	Mitochondrial outer membrane porin	P46274	107	12				–0.076	–0.486
B151	Malate dehydrogenase	C4J673	117	8				–0.162	0.489
B153	DNA-binding protein p24	A1YKH2	78	6				–0.225	–1.134
B160	Brain protein 44-like	Q6Z595	53	14				0.808	0.145
B161	Glutathione peroxidase chr01_pseudomolecule_IMGAG_V3	Medtr1g017	55	8				0.670	0.000
B161	Plastid ribosomal protein L11	Q8H8H8	80	10					
B162	Acid phosphatase, putative	Q9M4D6	87	7				0.047	–0.169
B163	Thaumatin-like protein	Q8S4P7	69	10				0.000	17.307
B166	Glutamate receptor 3 plant, putative	B9SDW1	57	2				14.689	15.459
B176	Pathogenesis-related protein 1	C3UZE2	200	28				0.000	16.427
B194	Peroxisomal (*S*)-2-hydroxy-acid oxidase (glycolate oxidase)	P05414	150	8				0.179	0.278
B205	Glucan endo-1,3-β-D-glucosidase	O82716	111	15				15.594	2.311
B206	β-1,3-Glucanase	Q4JH28	91	18				15.791	17.670
B209	Mitochondrial outer membrane porin	P46274	207	20				–0.062	–0.601
B216	Ribulose bisphosphate carboxylase large chain	Q3ZEK8	52	3				0.242	–1.044

The following spots, A714, A805, A806, A868, A888, A908, B002, B009, B011, B039, B041, B102, B114, B124, B152, B157, B193, B204, B207 and B210, revealed no matches. Statistical data are shown in Table S2. Further information (number of peptides, species, expected p//MW, SignalP and ChloroP results, etc.) are given in Table S3.

RBCL-binding protein subunits α and β isoforms (spots A251, A254, A259, A282–284), a 2-cysteine peroxiredoxin (spot A654), a psbR 10-kDa subunit of photosystem II (PSII, spot B098) and an RNA-binding protein (spot B112). This can only be explained as follows: (i) these proteins are encoded by chloroplastic genes, which consequently do not possess a cTP; or (ii) the hit sequence is incomplete. In our study, the total number of chloroplastic proteins reached 75 (53%), and most were acidic (57, 77%).

Metabolite profiling of wheat in response to SnToxA exposure

In addition to proteomics, we also performed an untargeted metabolomics approach in an attempt to understand the wheat response to SnToxA exposure. Gas chromatography-mass spectrometry (GC-MS) analysis was used to identify changes in polar primary metabolites in SnToxA-treated wheat leaf samples

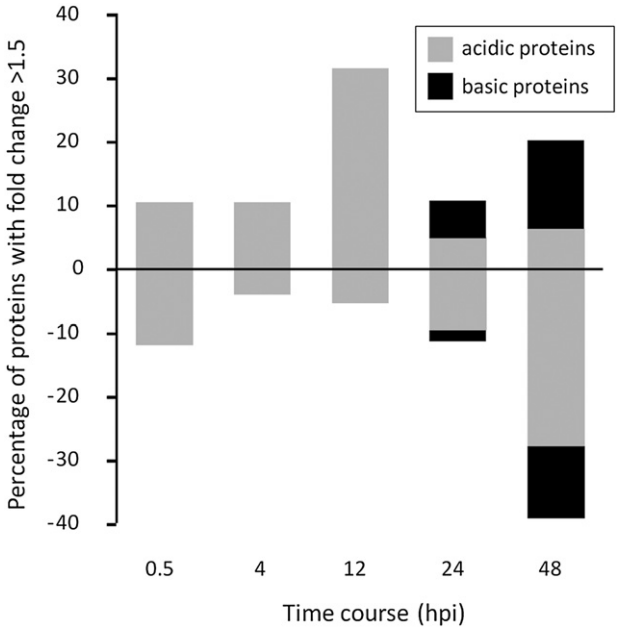

Fig. 3 Protein abundance in ToxA-infiltrated leaves relative to the controls over time. Up- and down-regulated (fold change >1.5, irrespective of *P* values) proteins were numbered and converted into a percentage; down-regulated proteins were converted to negative values using a −1 factor. Note that basic proteins were only analysed for the 24- and 48-h time points. hpi, hours post-infiltration.

throughout the 4–72-h time course after SnToxA infiltration. Principal component analysis (PCA) was used to discover trends within the split 20 : 1 dataset and to provide a means to observe the quality of the data. The six replicates belonging to each treatment and time point sampled clustered together, indicating the robustness and reproducibility of the experimental design. The first two principal components (PCs) explained 65% of the variance in the dataset (Fig. 4). PC1 accounted for 53% of the variance, which can largely be explained by the effect of time on metabolite changes, whereas the 12% of variance explained by PC2 clearly separates SnToxA-infiltrated wheat and control at 48 and 72 hpi. The samples can be divided into four clusters. The first contains the 4- and 12-h samples for both control and treated wheat. The second consists of all the 24-h samples. At 48 h, the variance as a result of metabolite changes between control and SnToxA-treated wheat becomes apparent. The third cluster contains the control 48- and 72-h samples, whereas the entire lower section of PCA is dominated by the fourth cluster grouping the SnToxA 48- and 72-h samples. The loadings plot (Fig. 4B) for this PCA illustrates the contribution of each metabolite to the variance between clusters. The metabolites with the highest contribution to PC1 are asparagine and four unknown compounds, and to PC2 are asparagine, quinic acid, malate and two unknown compounds.

ANOVA was performed to assess the statistical significance of the contribution of each metabolite to the variation between SnToxA and control wheat. The abundances of 92 metabolites detected using GC-MS were altered significantly ($P < 0.05$) by SnToxA. Of these, 32 were identified by a match to in-house databases and five were putatively identified with a match of above 80% to the NIST08 library or the Golm Metabolome Database (Table 2). The remaining 55 metabolites have not yet been identified (data not shown). A significant portion of these unidentified metabolites have fragmentation patterns indicative of sugars, which, by nature, are structurally very similar, and therefore in-house standards are required to provide accurate retention times for identification. Of the total 92 metabolites which responded significantly to SnToxA, approximately 60% displayed an increase in abundance at one or more time points, whereas the remainder decreased overall. An increase in metabolite abundance, particularly from 24 h, was the most noticeable trend observed in response to SnToxA, with 45%–60% of significant metabolites belonging to the three major groups of compounds (organic acids, sugar/sugar alcohols and unknowns) consistent with this pattern.

In addition to ANOVA, Student's *t*-test was performed on the 92 significantly different metabolites to identify those that were altered significantly by SnToxA at each individual time point ($P < 0.05$). Only the 37 identified using the databases mentioned previously are discussed here. At 4 hpi, 14 metabolites responded significantly to SnToxA treatment. Fructofuranoside was detected in SnToxA-treated leaves, but absent in the control, fructose was 1.8-fold lower in treated leaves and 2-*O*-glycerol-α-D-galactopyranoside was 1.9-fold higher. Another 10 unknown compounds had also responded to SnToxA treatment by this time point. Cluster 1 of PCA also included the 12-h samples, at which point 17 metabolites were altered significantly by SnToxA. Ribonic acid, xylitol, arabinitol, sedoheptulose and sucrose were all 1.2–1.6-fold lower in SnToxA-treated wheat. Glucuronic acid was detected in small amounts in the control, but absent in treated wheat, and glucose-6-phosphate and aspartic acid were detected in SnToxA-treated wheat, but were below the limits of detection in the control.

Cluster 2 of PCA grouped the 24-h control and SnToxA-treated samples. The 11 metabolites that were altered significantly in response to SnToxA at this point included α-ketoglutaric acid and glycerol, which were detected in the control, but absent in SnToxA-treated wheat. Glucuronic acid and glucaric acid, however, were present in SnToxA-treated wheat, but absent in the control.

At 48 and 72 hpi, the differences between SnToxA-treated wheat and the control became most prominent as they diverged into different clusters in PCA. This was reflected by the increase in the number of metabolites changing in response to SnToxA treatment. The abundance of 45 metabolites was altered significantly by SnToxA at 48 h, and that of 51 metabolites at 72 hpi. The compound 2-*O*-glycerol-α-D-galactopyranoside was a considerable 21-fold higher in abundance in SnToxA-treated wheat.

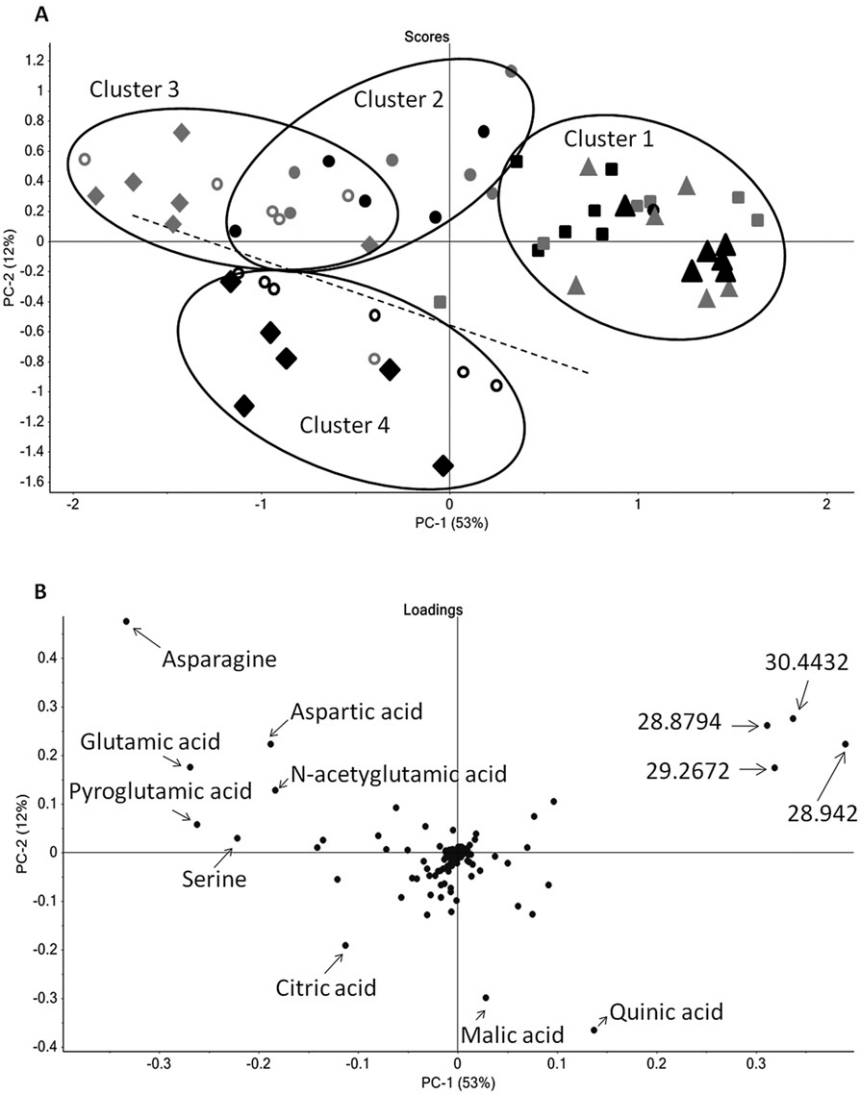

Fig. 4 (A) Score plots of principal component analysis (PCA) of gas chromatography-mass spectrometry (GC-MS) metabolite data for both control and SnToxA-infiltrated wheat leaves at five time points from 4 to 72 h post-infiltration (hpi). The symbols ■, ▲, ●, ○ and ◆ represent the time points 4, 12, 24, 48 and 72 hpi, respectively. SnToxA-treated samples are black and water-infiltrated control samples are grey. The numbers in parentheses indicate the variance in the datasets explained by the first two principal components (PCs). (B) Loadings plot illustrating the metabolites contributing to the variance observed in the PCA.

Threonic acid, fructose, γ-aminobutyric acid (GABA), malate, quinic acid and xylulose were amongst the known metabolites which also increased by more than two-fold in response to SnToxA at 48 h. At 72 h, 2-*O*-glycerol-α-D-galactopyranoside was still 13-fold higher in treated wheat. Quinic acid, fructofuranoside, threonic acid, malate, phosphoric acid, galactonic acid, glucuronic acid, fructose, erythronic acid and glyceric acid were also several fold higher in response to SnToxA. Those metabolites present at significantly lower abundances at 72 hpi in response to SnToxA included maltose, α-ketoglutarate, dehydroascorbic acid, asparagine and myo-inositol.

An absence of certain metabolites involved in the reactions of photosynthesis was noticeable in the GC-MS data. A number of low-molecular-weight metabolites, such as pyruvate and glyoxylate, are difficult to detect using standard GC parameters, and the majority of sugars were not detected in their phosphorylated forms because of instability in the conditions involved in this analysis. These facts highlight the benefits and complementary nature of undertaking both proteomics and metabolomics approaches.

DISCUSSION

SnToxA triggers the collapse of photosynthesis and causes an oxidative burst

The proteomics approach detected multiple proteins associated with PSI and PSII, as well as the Calvin cycle and other aspects of photosynthesis and photorespiration. The abundance of the majority of these proteins was observed to increase at 12 hpi with SnToxA, after which, they decreased significantly and continually in abundance throughout the remainder of the time course. It has been well established in previous studies that Ptr ToxA is targeted to the chloroplast and induces photosystem changes (Manning *et al*., 2007; Pandelova *et al*., 2009). These data suggest that

Table 2 Putatively identified metabolites differentially abundant in SnToxA-treated wheat.

		H_2O					ToxA				
Metabolite and ID	*	4 h	12 h	24 h	48 h	72 h	4 h	12 h	24 h	48 h	72 h
Amino acids											
L-Isoleucine_16.4189_1295_158_S	B	2.75 ± 1.38	1.06 ± 0.61	2.15 ± 0.85	2.62 ± 0.9	2.06 ± 0.73	0.95 ± 0.43	0.71 ± 0.31	ND	6.55 ± 2.39	6.21 ± 2.85
L-Glycine_16.7004_1307_174_S	A	11.07 ± 6.01	12.72 ± 7.56	ND	64.82 ± 22.86	66.2 ± 25.46	ND	6.64 ± 3.41	11.75 ± 6.49	22.08 ± 10.96	21.66 ± 8.15
Aspartic acid_21.7171_1522_232	B	9.44 ± 2.62	11.53 ± 4.11	26.24 ± 5.6	32.07 ± 11.75	51.8 ± 10.82	19.28 ± 3.09	6.42 ± 3	22.53 ± 4.97	22.63 ± 6.63	22.12 ± 4.98
Asparagine_24.8197_1692_116	C	11.22 ± 2.82	11.04 ± 7.46	64.67 ± 11.38	119.7 ± 40.45	150.3 ± 39.78	20.31 ± 5.27	2.5 ± 2.47	43.43 ± 10.59	28.84 ± 11.71	32.32 ± 15.15
Organic acids											
Glyceric acid_17.3134_1338_189	B	4.23 ± 0.85	1.93 ± 0.26	3.17 ± 0.23	2.76 ± 0.88	3.26 ± 1.05	4.31 ± 1.22	1.8 ± 0.3	2.07 ± 0.74	3.54 ± 1.21	7.66 ± 0.57
Malic acid_21.0415_1489_233	C	45.6 ± 3.66	32.85 ± 6.1	25.11 ± 3.2	19.49 ± 4.67	23.09 ± 1.67	52.03 ± 8.29	37.87 ± 4.17	29.35 ± 7.16	68.63 ± 7.1	101.1 ± 11.95
Pyroglutamic acid_21.7484_1524_156	B	43.42 ± 9.24	37.48 ± 10.58	105.9 ± 11.76	173.1 ± 32.22	145.9 ± 18.99	41.56 ± 5.26	16.5 ± 1.92	80.44 ± 14.96	91.84 ± 14.01	104.3 ± 15.91
GABA_21.911_1525_174_S	B	3.09 ± 1.08	1.16 ± 0.16	2.94 ± 0.88	3.38 ± 0.54	5.82 ± 1.12	2.08 ± 0.26	1.29 ± 0.3	2.15 ± 0.55	15.12 ± 2.94	9.6 ± 2.43
N-Acetylglutamic aid_22.0486_1540_84	B	3.44 ± 2.12	ND	15.9 ± 2.93	20.23 ± 6.66	36.03 ± 7.04	7.21 ± 1.08	ND	13.41 ± 2.23	17.53 ± 4.07	15.88 ± 6.05
Erythronic acid _22.1612_1547_292	C	0.18 ± 0.04	0.22 ± 0.05	0.17 ± 0.05	0.31 ± 0.02	0.44 ± 0.04	0.24 ± 0.01	0.18 ± 0.04	0.22 ± 0.05	0.6 ± 0.07	1.06 ± 0.05
Threonic acid_22.5428_1568_292	C	3.27 ± 0.21	2.73 ± 0.22	0.98 ± 0.1	0.85 ± 0.08	1.53 ± 0.22	2.48 ± 0.2	2.48 ± 0.2	1.09 ± 0.11	5.64 ± 0.76	11.09 ± 1.08
2-Ketoglutaric acid_22.9744_1591_198	B	0.29 ± 0.12	ND	0.47 ± 0.1	0.49 ± 0.11	0.71 ± 0.07	0.31 ± 0.07	ND	ND	0.51 ± 0.12	0.25 ± 0.11
Ribonic acid_26.3147_1774_333	C	0.32 ± 0.03	0.37 ± 0.02	0.39 ± 0.02	0.55 ± 0.04	0.59 ± 0.04	0.29 ± 0.02	0.31 ± 0.01	0.4 ± 0.02	0.65 ± 0.04	0.93 ± 0.04
Glyceric acid-3-phosphate_27.4032_1834_299	B	2.01 ± 0.32	ND	2.27 ± 0.32	3.43 ± 0.99	3.46 ± 1.16	1.96 ± 0.47	0.25 ± 0.12	3.1 ± 0.68	1.75 ± 0.41	0.89 ± 0.3
Citric acid_27.6096_1845_273	C	14.68 ± 1.89	22.53 ± 2.37	24.45 ± 3.52	35.18 ± 3.7	38.26 ± 2.37	17.2 ± 1.47	16.27 ± 1.03	27.4 ± 2.64	49.34 ± 4.13	70.48 ± 7.67
Dehydroascorbic acid_28.1038_1872_173	B	1.6 ± 0.77	1.84 ± 0.46	1.56 ± 0.17	2.13 ± 0.24	1.76 ± 0.14	0.81 ± 0.11	1.45 ± 0.66	1.17 ± 0.1	1.4 ± 0.18	0.7 ± 0.04
Quinic acid_28.2664_1881_345	C	91.78 ± 6	144.0 ± 13.86	36.44 ± 2.89	32.09 ± 4.1	30.37 ± 2.54	97.74 ± 5.72	140.0 ± 11.94	40.31 ± 5.58	102.0 ± 15.83	258.8 ± 17.67
Ascorbic acid_29.874_1970_332	B	6.54 ± 1.94	8.83 ± 1.22	18.06 ± 2.04	17.82 ± 1.97	21.18 ± 4.71	9.18 ± 1.44	7.65 ± 1.47	17.63 ± 1.36	13.05 ± 2.26	11.03 ± 2.54
Glucaric acid_30.8498_2023_333	C	0.61 ± 0.07	0.64 ± 0.06	ND	0.14 ± 0.07	ND	0.69 ± 0.05	0.77 ± 0.06	0.46 ± 0.17	0.45 ± 0.15	0.22 ± 0.11
Galactonic acid_30.9249_2027_292	C	0.12 ± 0.02	0.1 ± 0.01	0.06 ± 0.02	0.09 ± 0	0.05 ± 0.02	0.11 ± 0.01	0.08 ± 0.02	0.06 ± 0.02	0.14 ± 0.01	0.2 ± 0.03
Glucuronic acid_43.7858_2929_217	C	0.05 ± 0.02	0.06 ± 0.02	ND	0.1 ± 0.03	0.2 ± 0.02	0.12 ± 0.01	ND	0.09 ± 0.03	0.23 ± 0.05	0.72 ± 0.11
Sugars/sugar alcohols											
Erythritol_21.4106_1505_217	B	0.18 ± 0.04	0.28 ± 0.02	0.27 ± 0.01	0.34 ± 0.03	0.47 ± 0.05	0.19 ± 0.03	0.19 ± 0.02	0.19 ± 0.04	0.37 ± 0.02	0.66 ± 0.06
Xylose_24.6133_1681_103	B	0.78 ± 0.08	0.93 ± 0.09	0.45 ± 0.1	0.4 ± 0.1	0.58 ± 0.07	0.62 ± 0.05	0.78 ± 0.06	0.35 ± 0.12	0.25 ± 0.11	0.23 ± 0.14
Xylulose_24.9073_1697_205	B	1.79 ± 0.21	1.72 ± 0.18	1.22 ± 0.2	0.77 ± 0.2	1.1 ± 0.17	1.66 ± 0.26	1.85 ± 0.23	1.11 ± 0.27	1.65 ± 0.21	2.13 ± 0.27
Ribose_24.9198_1691_103_S	B	2.9 ± 0.4	2.67 ± 0.44	2.22 ± 0.55	0.76 ± 0.42	1.55 ± 0.49	2.81 ± 0.39	2.6 ± 0.22	2.38 ± 0.67	2.92 ± 0.6	3.52 ± 1.08
Arabinitol_25.7017_1741_217	B	0.25 ± 0.03	0.3 ± 0.04	0.28 ± 0.01	0.4 ± 0.03	0.4 ± 0.04	0.25 ± 0.03	0.2 ± 0.01	0.23 ± 0.06	0.34 ± 0.02	0.63 ± 0.07
Fructofuranoside_26.7776_1800_217	C	ND	0.2 ± 0.05	ND	0.44 ± 0.21	0.25 ± 0.16	0.2 ± 0.03	0.11 ± 0.03	0.19 ± 0.12	0.82 ± 0.08	1.84 ± 0.22
Fructose_28.5041_1894_103	C	51.5 ± 6.57	23.39 ± 2.79	13.04 ± 0.64	7.02 ± 2.39	10.97 ± 1.28	29.19 ± 1.8	16.91 ± 1.76	12.2 ± 1.7	36.41 ± 0.94	32.73 ± 5.89
Fructose {BP}_28.6855_1904_103	C	35.13 ± 5.18	16.36 ± 2.13	9.33 ± 0.5	7.26 ± 0.61	7.65 ± 1.02	21.52 ± 1.05	11.3 ± 1.24	8.66 ± 1.28	24.98 ± 0.73	21.96 ± 3.45
Galactose_28.8231_1912_319	B	1.54 ± 0.28	1.37 ± 0.1	0.75 ± 0.05	0.68 ± 0.07	0.63 ± 0.04	1.07 ± 0.08	1.09 ± 0.09	0.55 ± 0.15	0.94 ± 0.12	0.94 ± 0.05
Sedoheptulose_32.4637_2112_319	C	0.47 ± 0.03	0.81 ± 0.07	0.66 ± 0.04	1.33 ± 0.17	1.97 ± 0.21	0.48 ± 0.1	0.51 ± 0.05	0.56 ± 0.06	1.66 ± 0.08	3.48 ± 0.21
2-*O*-Glycerol-α-D-galactopyranoside_35.6539_2315_204	C	0.36 ± 0.12	0.42 ± 0.09	0.26 ± 0.13	0.51 ± 0.02	0.51 ± 0.1	0.69 ± 0.06	0.55 ± 0.04	0.63 ± 0.21	10.83 ± 1.31	6.51 ± 0.63
Glucose-6-phosphate_35.704_2319_387	C	0.74 ± 0.28	ND	0.25 ± 0.17	0.42 ± 0.14	ND	0.99 ± 0.23	0.52 ± 0.11	0.57 ± 0.19	1.05 ± 0.24	0.69 ± 0.32
Maltose_41.6402_2752_361	B	ND	0.45 ± 0.04	0.52 ± 0.04	0.66 ± 0.08	0.63 ± 0.06	0.09 ± 0.05	0.4 ± 0.1	0.36 ± 0.09	0.54 ± 0.06	0.17 ± 0.08
Isomaltose_41.7216_2758_204	B	ND	ND	ND	ND	0.18 ± 0.06	ND	ND	ND	0.24 ± 0.05	0.34 ± 0.11
Other											
Glycerol_15.8997_1280_205	A	ND	0.03 ± 0.01	0.04 ± 0.01	0.02 ± 0.01	0.03 ± 0.01	0.08 ± 0.04	0.06 ± 0.02	ND	0.03 ± 0.01	0.05 ± 0.02
myo-Inositol_32.176_2096_318	C	11.86 ± 1.63	10.13 ± 0.76	12.15 ± 0.76	13.48 ± 1.06	17.28 ± 1.19	10.93 ± 0.68	10.68 ± 0.83	13.85 ± 1.73	9.93 ± 1.34	8.91 ± 0.7

Metabolites are identified in the format 'name_retention time_retention index_base peak'. Metabolite abundances less than 0.01 are listed as not detected (ND). Data are primarily from 20 : 1 split gas chromatography-mass spectrometry (GC-MS) analysis; however, the abundance of a number of metabolites was calculated from splitless data and annotated with an '_S' extension to the metabolite ID. *Statistical significance (combination of treatment and treatment × time) as determined by analysis of variance (ANOVA) is indicated as A ($P < 0.05$), B ($P < 0.01$) or C ($P < 0.001$). A false discovery rate (FDR) method was applied.

SnToxA also appears to be localized and targeted to the chloroplast, where it has a negative impact on photosynthesis. How Ptr ToxA and SnToxA impair photosynthesis is currently unknown, although the binding of Ptr ToxA to plastocyanin has been demonstrated (Tai *et al*., 2007).

One of the primary outcomes of photosynthetic disruption is the accumulation of ROS. Previous studies on Ptr ToxA have demonstrated conclusively that its infiltration into Tsn1-wheat leaves results in the accumulation of ROS. Although ROS were not measured directly in this study, many enzymes associated with ROS detoxification and scavenging were identified as differentially abundant during SnToxA exposure. These included all three BAS1 peroxiredoxin isoforms, a chloroplastic lipocalin, a thioredoxin m, a glutathione peroxidase, a cyclophilin, as well as the peroxisome with an ascorbate peroxidase. The up-regulation of these ROS enzymes at 12 and/or 24 hpi implies that the cell and, in particular, the chloroplast actively detoxify ROS. The metabolomics data also provided evidence that the host is attempting to detoxify increasing ROS levels. This evidence includes increased levels of several metabolites associated with ascorbate metabolism, including dehydroascorbate, threonic acid, glucuronic acid and glucaric acid.

It is important to note that multiple sources of ROS in plant cells have been identified previously. The primary source for ROS produced in response to pathogen recognition is NAPDH oxidase. Evidence is also now emerging that ROS generated within the cell also plays a role in plant–pathogen interactions (Mur *et al*., 2008; Torres, 2010). Studies by Ciuffetti and co-workers have shown that ROS accumulate in the chloroplast of Ptr ToxA-treated leaves (Manning *et al*., 2009). One mechanism of ROS production in the chloroplast occurs when the photon intensity is in excess of that required for CO_2 fixation, also known as the excess excitation energy (EEE) (Karpinski *et al*., 2003). How exposure to SnToxA leads to EEE generation is unknown. One possibility may be the binding of SnToxA to plastocyanin, as has been demonstrated for Ptr ToxA. If SnToxA were to bind to, and inhibit, the function of plastocyanin, this would result in an accumulation of electrons in PSII, leading to the eventual degradation of the reaction centre (Schottler *et al*., 2004; Sommer *et al*., 2003). Perhaps the accumulation in the photosynthetic machinery demonstrated in this study at 12 hpi is a response by the cell to compensate for the initial decrease in efficiency caused by the binding of SnToxA to plastocyanin. This compensatory increase, however, would be finite, and the continual blockage of electron transfer between the two photosystems through the binding of SnToxA to plastocyanin would eventually lead to excessive electron accumulation, triggering the collapse of the photosystems. This is evident from the continual decrease in proteins involved in both photosynthesis and photorespiration throughout the later periods of the time course. It is also relevant that the abundance of enzymes associated with ROS detoxification decreased significantly after 24 hpi. These data suggest that the scavenging and detoxification of ROS are probably overwhelmed by the levels produced through the collapse of photosynthesis, leading to the continual increase in ROS levels during exposure, as reported previously.

The roles of ROS produced in the chloroplast in response to SnToxA exposure are likely to be multiple. First, it is well established that lipid peroxidation by H_2O_2 plays a key role in the execution of light-dependent cell death (Montillet *et al*., 2005; Torres, 2010). Apart from the requirement of SnToxA for light, our data also show a strong up-regulation of chloroplastic lipocalin. Chloroplastic lipocalin is a thylakoid luminal protein that responds positively at the transcriptional level to various abiotic stresses, including drought, high light and paraquat (Levesque-Tremblay *et al*., 2009). Mode-of-action studies have shown that it is involved in the protection of thylakoid membranes from lipid peroxidation (e.g. as a product of photosynthetic impairment) and that it represents a defence mechanism against oxidative stress. It has also been demonstrated that ROS have regulatory and signalling roles, including the induction of phosphorylation cascades involved in cell death responses (Asai *et al*., 2002; Samuel *et al*., 2005; Torres, 2010). It is significant to note that Pandelova *et al*. (2009) showed the up-regulation of TaMPK3 gene expression during Ptr ToxA exposure, particularly towards the latter stages of the time course study when ROS levels would be at their highest. MPK3 homologues are mitogen-activated protein (MAP) kinases that have been shown to respond positively at the transcriptional, translational and post-translational levels during the activation of either effector-triggered immunity or pathogen-associated molecular pattern (PAMP)-triggered immunity. Rudd *et al*. (2008) have shown that TaMPK3 responds to infection by the related wheat pathogen *Mycosphaerella graminicola*, and have suggested that it plays a role in ETS. The current study and previous observations suggest that ROS induced by SnToxA and Ptr ToxA localization to the chloroplast are involved directly in cell death through lipid peroxidation, and also act as signalling molecules to trigger the ETS response.

SnToxA induces host defence responses

Biomarkers commonly observed during pathogen invasion showed a response to SnToxA infiltration, in particular pathogenesis-related (PR) proteins, including cell wall-degrading enzymes. Also known as inducible defence-related proteins, PR proteins are absent or barely detectable in healthy tissues, and accumulate under pathological conditions. Although not categorized as a PR protein, a phenylalanine ammonia-lyase, the first enzyme of the phenylpropanoid pathway, falls within this definition (Van Loon *et al*., 2006). All of the ten PR proteins identified in this study were significantly ($P < 0.05$) more abundant in SnToxA-infiltrated leaves at 48 hpi than in controls. Nine were basic and were induced by more than 3.8-fold; there were four chitinases (spots B024, B038, B116, B119), which could belong to the PR-3, PR-4, PR-8 or PR-11 family, two thaumatin-like proteins (spots B023, B163), part of the

PR-5 family, one member of the PR-1 family (spot B176) and two β-glucosidases (spots B205, B206), members of the PR-2 family. The acidic β-glucosidase (spot A550) was up-regulated in SnToxA-infiltrated leaves at 0.5, 4 and 48 hpi, by 2.5-, 2.6- and 2.3-fold, respectively. At 48 hpi, phenylalanine ammonia-lyase (B046) presented a 2.7-fold significant ($P < 0.01$) induction at the protein level. Previous studies have demonstrated that the transcript levels of chitinase, a PR-1 protein and β-glucosidase (Adhikari *et al*., 2009), as well as the transcript abundances of PR-2 and PR-4 proteins (Pandelova *et al*., 2009), increase in wheat leaves infiltrated with Ptr ToxA. It is interesting to note that no PR proteins were detected as being differentially abundant in a recent study examining the effect of PtrToxB on the wheat leaf proteome (Kim *et al*., 2010). Most PR proteins possess antifungal properties. Although the mode of action and cellular and molecular targets of PR-1 remain unknown, its involvement in the host defence reaction against a variety of pathogens has been widely reported; moreover, its constitutive or over-expression leads to an enhanced host resistance or tolerance (Van Loon *et al*., 2006). Both chitinases and β-glucosidases hydrolyse glycosidic bonds in fungal cell walls, thereby releasing chitin oligomers and β-1,3-glucans, respectively, which, in turn, act as elicitors of the defence reaction. Resistance in wheat would rely on a rapid recognition of the fungal pathogen sensed from released β-1,3-glucans (Shetty *et al*., 2009). Similarly, thaumatin-like proteins are assumed to destroy the fungal cell wall through glucan binding and glucanase activities (Liu *et al*., 2010).

The interesting aspect of this observed increase in PR protein abundance on SnToxA exposure is that it occurs in the absence of the pathogen or any other known PAMPs. A previous study examining PR protein gene expression in catalase-deficient tobacco showed conclusively that sublethal levels of H_2O_2 were sufficient to activate the expression of acidic and basic PR proteins. However, it was the onset of chlorosis and necrosis (as observed in a typical HR response) that was the trigger for rapid and strong activation of PR protein expression (Chamnongpol *et al*., 1998). Evidence from this study and others has shown that Ptr ToxA and SnToxA exposure results in the induction of intracellular ROS production and the up-regulation of ROS-detoxifying enzymes. It is significant to note that PR proteins begin to accumulate at 24 hpi, but increase significantly at 48 hpi, precisely the time at which the visible symptoms of chlorosis become apparent. Taken together, these data imply that the accumulation of ROS, including H_2O_2, as a result of the disruption of the photosynthetic process, is sufficient to cause an increase in PR protein abundance in the absence of *S. nodorum*.

SnToxA has significant effects on central primary metabolism

Using a complementary metabolomics approach, this study has shown that SnToxA exposure results in significant consequences on the central carbon metabolism of wheat. It should be considered that, although the measurement of differentially expressed transcripts and protein levels provides some indication of metabolic control, changes in protein abundance do not always correlate with enzymatic activity, which is often controlled by the substrates and products themselves. Many reactions are controlled at the post-translational level involving metabolic feedback mechanisms and phosphorylation (Paul and Pellny, 2003). A key example of this concept is the inhibition of phosphofructokinase [PFK, a principal regulator of the carbon flux through glycolysis and the tricarboxylic acid (TCA) cycle] by phosphoenolpyruvate, a downstream product of the reaction catalysed by PFK (Berg *et al*., 2007). Analysis of the small polar metabolome has demonstrated that SnToxA causes significant changes in the abundance of TCA cycle intermediates at the stage of visible plant chlorosis. The TCA cycle serves the crucial role of producing usable energy to the cell in the form of ATP, in addition to generating the reducing power essential for many biochemical reactions (Fernie *et al*., 2004). Interestingly, two key intermediates in this pathway (citrate and malate) show a significant increase in abundance from 48 hpi in response to SnToxA (fold changes of 1.8 and 4.4, respectively, at 72 hpi). Succinate, although not significant ($P = 0.07$ at 48 h), is also consistent with this trend. The proteomics data generated in this study substantiate the claim, with data detailing a late induction of the TCA cycle enzyme malate dehydrogenase (MDH) in response to SnToxA treatment. This enzyme has been shown previously to be up-regulated in wheat in response to the proteinaceous effector PtrToxB (Kim *et al*., 2010).

The up-regulation of TCA cycle intermediates on SnToxA exposure appears to belie the chlorotic state of the infiltrated host tissue at this stage. It has been demonstrated that the gene expression of TCA cycle enzymes in *Arabidopsis thaliana* increases in response to the bacterial plant pathogen *Pseudomonas syringae* (Scheideler *et al*., 2002). We present the first direct evidence of an increase in TCA cycle metabolites in response to pathogen effectors. It could be speculated that the up-regulation of TCA cycle metabolism is a consequence of the inhibition of photosynthesis caused by SnToxA. Ptr ToxA causes chlorophyll loss (Manning *et al*., 2004) and decreases in photosystem complexes I and II (Adhikari *et al*., 2009; Pandelova *et al*., 2009), disrupting the electron transport chain (ETC) and therefore energy production in chloroplasts. The ETC in mitochondria is therefore the only remaining site for energy production to continue. The mitochondrial ETC requires an electron donor, which can be generated by the TCA cycle in the form of NADPH (Buchanan *et al*., 2009). However, the lack of the ability of plants to photosynthesize following SnToxA treatment reduces the availability of sugars for conversion to acetyl-CoA required for the TCA cycle to function. In such conditions of starvation, β-oxidation of fatty acids is often utilized to generate acetyl-CoA (Graham *et al*., 1994).

In plants, β-oxidation of fatty acids occurs in glyoxysomes (Cooper and Beevers, 1969). The acetyl-CoA produced is used in the glyoxylate cycle, which bears similarities to the TCA cycle; however, the two CO_2-producing steps are omitted (Berg *et al*., 2007). The majority of research concerning the role of the glyoxylate cycle in plants has been undertaken on germinating seeds and senescing leaves (Graham *et al*., 1994; McLaughlin and Smith, 1994), as this pathway was, until recently, considered to be redundant once plants are able to photosynthesize. However, mature plants, including wheat, have been shown to possess the enzymes involved in this cycle (Janssen, 1995; Nieri *et al*., 1997; Pistelli *et al*., 1991). Several studies have observed glyoxylate cycle activation during the HR induced by fungal invasion (Cots *et al*., 2002) and under conditions of starvation (Graham *et al*., 1992, 1994). β-Oxidation of fatty acids and carbon metabolism through the glyoxylate cycle represent a possible mechanism for enabling wheat to continue energy production following SnToxA treatment. In support of the glyoxylate cycle hypothesis, the only TCA cycle intermediate detected in this study that did not follow a pattern of increasing abundance was α-ketoglutarate, a metabolite bypassed in the glyoxylate cycle.

A further explanation for the up-regulation of the TCA cycle is the synthesis of metabolites, such as amino acids and porphyrins, which, apart from having important roles themselves, are building blocks for secondary metabolites important in plant defence (Buchanan *et al*., 2009). Studies are currently underway to analyse the secondary metabolites in SnToxA-treated samples. An example of a primary metabolite synthesized by the TCA cycle is GABA, a nonprotein amino acid well known for its role as a neurotransmitter in animals (Bouche and Fromm, 2004). GABA accumulates in response to abiotic and biotic stresses; however, it has an enigmatic role in plants and, only recently, has research identified its part in the carbon–nitrogen balance, regulation of pH, herbivore defence, redox regulation, energy production and as a signalling molecule (Fait *et al*., 2008; Oliver and Solomon, 2004; Solomon and Oliver, 2002). GABA has also been reported to prevent damage caused by oxidative stress as reducing equivalents are produced by the GABA shunt to eliminate ROS (Oliver and Solomon, 2004). GABA was present at significantly higher abundance at 48 and 72 hpi in response to SnToxA treatment. Its precursor, α-ketoglutarate, showed a decrease at 72 hpi in SnToxA-treated wheat, suggesting depletion, perhaps as a result of the production of glutamate and, subsequently, GABA. Whether GABA is produced in response to oxidative stress or as a signalling molecule has yet to be established.

SnToxA and Ptr ToxA have comparable modes of action

A previous seminal study by Friesen *et al*. (2006) demonstrated that SnToxA, like Ptr ToxA, interacts with Tsn1. This is the first such study to analyse the host response to SnToxA exposure and, as such, has allowed us to further assess the relationship of Ptr ToxA and SnToxA in terms of biological activity. The data presented in this study show that SnToxA appears to cause significant effects on photosynthesis, with many proteins associated with this process significantly less abundant after a short exposure to the effector protein. SnToxA also induces a series of defence responses in susceptible wheat leaves, including the up-regulation of multiple PR proteins and significant changes to ROS metabolism. These changes have mostly been described for Ptr ToxA-infiltrated leaves, albeit at the transcript level, demonstrating, for the first time, the comparable nature of SnToxA and Ptr ToxA in terms of biological activity.

These data also provide further evidence that necrotrophic pathogens, such as *S. nodorum* and *P. tritici-repentis*, seek to manipulate existing host machinery to cause cell death and promote infection. However, many questions still remain, in particular with respect to the roles of the generated ROS, and follow-up work is now underway to examine host signalling pathways and lipid composition during SnToxA exposure. It is also worth noting that a further two genes encoding effector proteins in *S. nodorum* have been identified recently (Liu *et al*., 2009). This study has highlighted the power of investigating both proteins and metabolites during effector exposure, and it is envisaged that such approaches will be employed to analyse the modes of action of these two new necrotrophic effectors.

EXPERIMENTAL PROCEDURES

Wheat culture, leaf infiltration and sampling, and toxicity assay

SnToxA-sensitive wheat (*Triticum aestivum* L. genotype BG261) was grown from seeds, as described previously (Solomon *et al*., 2006). SnToxA was purified from *S. nodorum*, as described previously (Oliver *et al*., 2009). Ten-day-old plants were infiltrated, as described previously (Liu *et al*., 2004), with either distilled H_2O or purified SnToxA (1.22 μg/mL) at the start of the photoperiod.

Plants for proteomic analysis were collected at 0, 0.5, 4, 12, 24 and 48 hpi. Three biological replicates were collected, each containing ten infiltrated areas. Infiltrated leaf areas for soluble protein extraction were pooled and instantly frozen in liquid nitrogen and stored at −80 °C. Plants for metabolomic analysis were harvested at 0, 4, 12, 24, 48 and 72 hpi. Six biological replicates were harvested, each containing eight leaf sections per sample. Metabolism was quenched in liquid nitrogen immediately and tissue was stored at −80 °C until extraction.

For the toxicity assay, fresh infiltrated leaf samples were digitalized using a flatbed scanner (model Epson Perfection 4990 Photo, Epson, North Ryde, NSW, Australia). Changes in colour associated with infiltration symptoms were analysed using Scion Image software (Scion Corporation, Frederick, MD, USA) following the method devised by Wijekoon *et al*. (2008). The chlorotic area associated with SnToxA infiltration was quantified across the following time course: 0, 0.5, 4, 12, 24, 48 and 72 hpi (Adhikari

et al., 2009). Five leaves infiltrated with water and ten leaves infiltrated with SnToxA were used for each time point.

Protein extraction, assay and labelling

Frozen leaf samples were finely ground in liquid nitrogen using a chilled mortar and pestle. Soluble proteins were extracted using a trichloroacetic acid–2-mercaptoethanol–acetone method devised by Damerval *et al*. (1986). Protein pellets were solubilized in 1 mL DIGE lysis buffer (7 M urea, 2 M thiourea, 4% w/v 3-[3-(cholamidopropyl)dimethylammonio]-1-propanesulphonate, 30 mM Tris-Cl, pH 8.5). Protein extracts were transferred into 2-mL Eppendorf tubes and their pH was monitored by diluting 2 μL into 20 μL double-distilled H_2O and wetting pH 0–14 indicator strips (Merck, Kilsyth, Vic., Australia). When necessary, the pH of the protein extract was adjusted to 8.5 with 50 mM NaOH.

The protein content of leaf protein extracts was estimated using a 2-D Quant Kit (GE Healthcare, Ryldamere, NSW, Australia) following the manufacturer's instructions. Protein extracts were stored at –20 °C until use.

In order to maximize labelling reproducibility across samples, a 150-μg aliquot of each protein extract was transferred into a fresh 1.5-mL Eppendorf tube and completed with DIGE lysis buffer to bring the volume to 150 μL in each tube. The homogeneity of protein content was further checked using one-dimensional electrophoresis (data not shown). Samples were labelled using CyDye DIGE fluors (minimal dyes kit, GE Healthcare), according to the manufacturer's instructions, with minor modifications. Amine reactive cyanine (Cy) dyes were freshly dissolved in anhydrous dimethyl formamide. The internal standard consisted of a pool of 75 μg of each sample and was labelled with 200 pmol Cy2. DIGE labels were assigned to samples according to a randomized design; 150 μg of proteins of each sample were labelled with 200 pmol Cy3 or Cy5. Labelling reactions were performed in a cold room on ice and quenched using 10 mM lysine. Samples labelled with Cy3 and Cy5 were randomly pooled and mixed with the Cy2-labelled internal standard prior to isoelectric focusing (IEF). The labelling reaction was incubated on ice in the dark for 30 min. The reaction was terminated by the addition of 10 nmol lysine.

Two-dimensional electrophoresis

Wheat leaf proteins were separated using two-dimensional electrophoresis (O'Farrell, 1975). During the first dimension, proteins were resolved along two pH ranges: acidic (pH 4–7) and basic (pH 7–10); they are hereafter referred to as acidic and basic proteins, respectively.

For acidic proteins, all 36 samples (two treatments × six time points × three replicates) were analysed over the whole 0–48-h time course. DIGE-labelled protein samples were separated using the IPG-IEF technique (Bjellqvist *et al*., 1982). Pooled labelled samples (375 μg proteins/gel) were diluted into an IEF solution (7 M urea, 2 M thiourea, 4% w/v 3-[3-(cholamidopropyl)dimethylammonio]-1-propanesulphonate, 1% w/v dithiothreitol, 1% v/v 2-mercaptoethanol, 10 mM tris-(2-carboxyethyl)-phosphine-HCl, 0.25% ampholites 3–10, 0.25% ampholites 4–7) to reach a volume of 470 μL, and then loaded onto 24-cm 4–7 IPG strips (GE Healthcare) through in-gel rehydration. IPG-IEF was performed at 20 °C using IPGphor II (GE Healthcare) and the following programme: 0 V for 1 h, after which mineral oil was added, 50 V for 12 h, 200 V for 30 min, 500 V for 30 min, 1000 V for 1 h, 8000 V for 90 h, until a total of 93 000 Vh had passed.

For basic proteins, 12 samples (two treatments × two time points × three replicates) from time points 24 h and 48 h were separated using IPG-IEF. Unlabelled protein samples (500 μg proteins/gel) were diluted into DeStreak rehydration solution (GE Healthcare) with 1% ampholites 7–10 to reach a volume of 470 μL, and then loaded onto 24-cm 7–10 IPG strips (Bio-Rad, Hercules, CA, USA) through passive in-gel rehydration overnight. IPG-IEF was performed at 20 °C using MultiPhor II (GE Healthcare) and the following programme: 150 V for 15 min, 200 V for 30 min, 300 V for 5 min, 300 V for 5 h, 1000 V for 5 h, 3500 V for 4 h, 3500 V for 102 h, until a total of 370 000 Vh had passed. To produce gels for spot excision, the same protocol was applied, except that 1 mg of proteins was loaded.

IPG strip equilibration was performed according to Görg *et al*. (1988) by incubation in 1% dithiothreitol for 15 min, followed by incubation in 2.5% iodoacetamide for 15 min. Equilibrated IPG strips were transferred onto 12.5% homecast polyacrylamide/bisacrylamide (37.5 : 1) gels (0.1 × 24 × 20 cm^3) and sealed in 1% (w/v) agarose (Invitrogen, Mulgrave Vic., Australia) in Laemmli (Laemmli, 1970) running buffer with 0.002% (w/v) bromophenol blue (BPB). The second dimension was performed using the Ettan DALT*six* Electrophoresis Unit (GE Healthcare) at 10 °C at 40 V for 30 min, followed by 450 V for 4 h 30 min (0.4 mA, 100 W).

Gel staining, image processing and statistical analyses

For labelled acidic proteins, two-dimensional gels were digitalized using Typhoon Trio (GE Healthcare) employing fluorescence acquisition mode, 200-μm resolution, 600 V photomultiplier tube and normal sensitivity. Images were analysed using DeCyder 2D 7.0 (GE Healthcare). About 1000 spots were detected per image.

For basic proteins, two-dimensional gels were stained following the silver nitrate staining method developed by Rabilloud and Charmont (2000). Stained gels were scanned using a Molecular Imaging PharosFX Plus system (Bio-Rad) at 100-μm resolution with the densitometry mode. Images were converted into *TIF* format (16-bit greyscale, 254 dots per inch). Images were processed using ImageMaster 2D Platinum (GE Healthcare). About 500 spots were detected per image. Statistical analyses were executed on reproducible spots only (i.e. present in two of three biological replicates).

Two-way ANOVAs were performed using JMP 8.0.1 software (SAS Institute Inc., Cary, NC, USA) and the following model: $A_{ij} = TI_i + TR_j + (TI \times TR)_{ij} + e_{ij}$, where A_{ij} denotes the protein abundance measured for time i and treatment j, with $1 < i < 6$ and $1 < j < 2$. The terms TI_i and TR_j measure the effect of the time and treatment, respectively. The interaction term $(TI \times TR)_{ij}$ accounts for the interaction between time and treatment. An FDR method (Reiner *et al*., 2003) was applied. One-way ANOVAs were also carried out using JMP at each time point, employing the following model: $A_i = TR_i + e_i$, where A_i denotes the protein abundance measured for treatment i, with $1 < i < 2$. All spots that displayed significant P values ($\alpha = 0.1$) for treatment and time × treatment interaction effects were selected for excision. Among the spots that displayed significant P values for the time effect, those that showed significant treatment effect at a particular time point were also selected for excision. Hierarchical clustering analyses (HCAs) using Ward's method and PCAs were performed using JMP.

For the excision of significant acidic spots, two-dimensional gels obtained following DIGE labelling and separation along the pH 4–7 range

were further stained using the 'Blue Silver' Coomassie staining protocol of Candiano *et al*. (2004). For the excision of significant basic spots, two-dimensional gels on which 1 mg of proteins from pooled samples per time point (24 and 48 h) were loaded and resolved along the pH 7–10 range were stained following Candiano *et al*. (2004).

Protein identification using MS

Significant spots (76 acidic and 54 basic) were manually excised in duplicate from Coomassie-stained gels and pooled into a fresh tube. Following destaining by three 45-min washes with 25 mM ammonium bicarbonate in 50 : 50 acetonitrile–water, spots were vacuum dried, trypsin digested and analysed using a 5800 MALDI TOF/TOF TM analyser (Applied Biosystems/MDS SCIEX, Mulgrave, Vic., Australia) as described in Bringans *et al*. (2008a). The 55 spots that did not yield any spectrum were further analysed using a Ultimate 3000 nanoflow LC system (Dionex, Bannockburn, IL, USA) online with the 4000-Q-Trap (Applied Biosystems), as described in (Bringans *et al*., 2008b).

Peptide mass fingerprinting spectra and the peptide sequence spectra of each sample were processed using MASCOT software (Matrix Science, London, UK) hosted at the Australian Proteomics Computational Facility (http://www.apcf.edu.au). MASCOT parameters were set as follows: methionine oxidation as a variable modification, one maximum miscleavage, monoisotopic 1+ peptide charge and a 0.4-Da peptide tolerance. Data search files were searched against the nonredundant (nr) National Center for Biotechnology Information (NCBI) database restricted to Viridiplantae. MS outputs are available on the PRIDE repository (http://www.ebi.ac.uk/pride) with accession number 16648, corresponding to spots A136 to B216. These outputs are also available in Table S4 (see Supporting Information).

The TargetP algorithm (Emanuelsson *et al*., 2000) (http://www.cbs.dtu.dk/services/TargetP/) was used online to predict targeted compartments. The ChloroP algorithm (Emanuelsson *et al*., 1999) (http://www.cbs.dtu.dk/services/ChloroP/) was used online to predict chloroplast targeting based on the predicted presence of cTP. Proteins of unknown function were further searched against the nr database using the BLASTp algorithm. Annotations with a minimum *E* value of 1.00e-25 were selected; their abbreviated codes display an asterisk.

Extraction, derivatization and analysis of wheat metabolites using GC-MS

Metabolite analysis was carried out with slight modifications to previous methods (Ipcho *et al*., 2010). Sample weights were taken of frozen tissue before samples were homogenized (2 min, 20 Hz) in a Tissue Lyser (Qiagen, Hilden, Germany). Frozen tissue powder (approximately 60 mg) was extracted with methanol (800 μL) containing 0.125 mg/mL of ribitol internal standard. The mixture was extracted at 4 °C with shaking (45 min, 900 rpm) and mixed with water (200 μL). To remove nonpolar metabolites, chloroform (500 μL) was added, mixed vigorously and centrifuged (10 min, 2000 ***g***). The upper methanol–water phase was taken and washed again with chloroform (500 μL). The nonpolar phase was discarded and the methanol–water phase was dried under vacuum.

Derivatization was performed online with the Gerstel MultiPurpose Sampler (Linthicum, MD, USA). Methoximation of carbonyl groups was achieved with incubation and shaking at 37 °C (90 min, 1200 rpm) with methylamine-HCl (20 μL, 20 mg/mL in pyridine). Trimethylsilylation of polar groups was completed by the addition of 30 μL of *N*-trimethylsilyl-*N*-methyl trifluoroacetamide (MSTFA), followed by incubation at 37 °C and shaking for 30 min.

GC-MS analysis was undertaken as described previously (Lowe *et al*., 2009). Samples were analysed in splitless and 20 : 1 split modes in order to obtain quantitative data for all metabolites over the extensive range of concentrations present. The splitless dataset was used for metabolites of lower concentration which were not reliably quantified in the split analysis. Metabolite abundances were normalized to the ribitol internal standard and sample weights using AnalyzerPro (SpectralWorks Ltd., Runcorn, Cheshire, UK). The mass spectra of the compounds found were identified using the publicly available Golm metabolome database (Max-Planck-Institute for Plant Physiology; Schauer *et al*., 2005) and the commercial National Institute of Standards and Technology 08 (NIST; http://www.nist.gov/index.html) mass spectral library. Data analyses were carried out using The Unscrambler (Version 10.0, CAMO ASA, Oslo, Norway) and the JMP 8.0.1 statistical package (SAS Institute Inc.). Metabolites deemed to be significant as determined by ANOVA for treatment and treatment × time were combined. An FDR method was applied (Benjamini and Hochberg, 1995).

ACKNOWLEDGEMENTS

We thank Sue Lyons for her help with growth chamber parameters, Rosemary Birch, Melanie Wagner and Liam Cassidy for their help with leaf infiltration, Samira Hassan for her assistance with Typhoon, Cassandra Harris for her assistance with DeCyder and Dr Michael Djordjevic for the use of ImageMaster2D. This work was financially supported by the Australian Research Council (DP0986139).

REFERENCES

Adhikari, T.B., Bai, J., Meinhardt, S.W., Gurung, S., Myrfield, M., Patel, J., Ali, S., Gudmestad, N.C. and Rasmussen, J.B. (2009) Tsn1-mediated host responses to ToxA from *Pyrenophora tritici-repentis*. *Mol. Plant–Microbe Interact.* **22**, 1056–1068.

Asai, T., Tena, G., Plotnikova, J., Willmann, M.R., Chiu, W.L., Gomez-Gomez, L., Boller, T., Ausubel, F.M. and Sheen, J. (2002) Map kinase signalling cascade in Arabidopsis innate immunity. *Nature*, **415**, 977–983.

Ballance, G.M., Lamari, L. and Bernier, C.C. (1989) Purification and characterization of a host-selective necrosis toxin from *Pyrenophora tritici-repentis*. *Physiol. Mol. Plant Pathol.* **35**, 203–213.

Benjamini, Y. and Hochberg, Y. (1995) Controlling the false discovery rate: a practical and powerful approach to multiple testing. *J. R. Stat. Soc. Ser. B (Methodol.)* **57**, 289–300.

Berg, J.M., Tymoczko, J.L. and Stryer, L. (2007) *Biochemistry*. New York: W.H. Freeman and Company.

Bjellqvist, B., Ek, K., Righetti, P.G., Gianazza, E., Gorg, A., Westermeier, R. and Postel, W. (1982) Isoelectric focusing in immobilized pH gradients: principle, methodology and some applications. *J. Biochem. Biophys. Methods*, **6**, 317–339.

Bouche, N. and Fromm, H. (2004) GABA in plants: just a metabolite? *Trends Plant Sci.* **9**, 110–115.

Bringans, S., Eriksen, S., Kendrick, T., Gopalakrishnakone, P., Livk, A., Lock, R. and Lipscombe, R. (2008a) Proteomic analysis of the venom of *Heterometrus longimanus* (Asian black scorpion). *Proteomics*, **8**, 1081–1096.

Bringans, S., Kendrick, T.S., Lui, J. and Lipscombe, R. (2008b) A comparative study of the accuracy of several de novo sequencing software packages for datasets derived by matrix-assisted laser desorption/ionisation and electrospray. *Rapid Commun. Mass Spectrom.* **22**, 3450–3454.

Buchanan, B.B., Gruissem, W. and Jones, R.L. (2009) *Biochemistry and Molecular Biology of Plants*. Somerset, NJ: John Wiley & Sons Inc.

Candiano, G., Bruschi, M., Musante, L., Santucci, L., Ghiggeri, G.M., Carnemolla, B., Orecchia, P., Zardi, L. and Righetti, P.G. (2004) Blue silver: a very sensitive colloidal Coomassie G-250 staining for proteome analysis. *Electrophoresis*, **25**, 1327–1333.

Chamnongpol, S., Willekens, H., Moeder, W., Langebartels, C., Sandermann, H., Van Montagu, M., Inze, D. and Van Camp, W. (1998) Defense activation and enhanced pathogen tolerance induced by H_2O_2 in transgenic tobacco. *Proc. Natl. Acad. Sci. USA*, **95**, 5818–5823.

Cooper, T.G. and Beevers, H. (1969) Mitochondria and glyoxysomes from castor bean endosperm. Enzyme constituents and catalytic activity. *J. Biol. Chem.* **244**, 3507–3513.

Cots, J., Fargeix, C., Gindro, K. and Widmer, F. (2002) Pathogenic attack and carbon reallocation in soybean leaves (*Glycine max* L.): reinitiation of the glyoxylate cycle as a defence reaction. *J. Plant Physiol.* **159**, 91–96.

Damerval, C., de Vienne, D., Zivy, M. and Thiellement, H. (1986) Technical improvements in two-dimensional electrophoresis increase the level of genetic variation detected in wheat-seedling proteins. *Electrophoresis*, **7**, 52–54.

Emanuelsson, O., Nielsen, H. and Von Heijne, G. (1999) ChloroP, a neural network-based method for predicting chloroplast transit peptides and their cleavage sites. *Protein Sci.* **8**, 978–984.

Emanuelsson, O., Nielsen, H., Brunak, S. and Von Heijne, G. (2000) Predicting subcellular localization of proteins based on their N-terminal amino acid sequence. *J. Mol. Biol.* **300**, 1005–1016.

Fait, A., Fromm, H., Walter, D., Galili, G. and Fernie, A.R. (2008) Highway or byway: the metabolic role of the GABA shunt in plants. *Trends Plant Sci.* **13**, 14–19.

Faris, J.D., Anderson, J.A., Francl, L.J. and Jordahl, J.G. (1996) Chromosomal location of a gene conditioning insensitivity in wheat to a necrosis-inducing culture filtrate from *Pyrenophora tritici-repentis*. *Phytopathology*, **86**, 459–463.

Faris, J.D., Zhang, Z., Lu, H., Lu, S., Reddy, L., Cloutier, S., Fellers, J.P., Meinhardt, S.W., Rasmussen, J.B., Xu, S.S., Oliver, R.P., Simons, K.J. and Friesen, T.L. (2010) A unique wheat disease resistance-like gene governs effector-triggered susceptibility to necrotrophic pathogens. *Proc. Natl. Acad. Sci. USA*, **107**, 13 544–13 549.

Fernie, A.R., Carrari, F. and Sweetlove, L.J. (2004) Respiratory metabolism: glycolysis, the TCA cycle and mitochondrial electron transport. *Curr. Opin. Plant Biol.* **7**, 254–261.

Flor, H.H. (1942) Inheritance of pathogenicity in *Melampsora lini*. *Phytopathology*, **32**, 653–669.

Flor, H.H. (1956) The complementary systems in flax and flax rust. *Adv. Genet.* **8**, 29–54.

Friesen, T.L., Stukenbrock, E.H., Liu, Z., Meinhardt, S., Ling, H., Faris, J.D., Rasmussen, J.B., Solomon P.S., McDonald B.A. and Oliver R.P. (2006) Emergence of a new disease as a result of interspecific virulence gene transfer. *Nat. Genet*, **38**, 953–956.

Friesen, T.L., Faris, J.D., Solomon, P.S. and Oliver, R.P. (2008) Host-specific toxins: effectors of necrotrophic pathogenicity. *Cell. Microbiol.* **10**, 1421–1428.

Görg, A., Postel, W., Gunther, S. and Friedrich, C. (1988) Horizontal two-dimensional electrophoresis with immobilized pH gradients using PhastSystem. *Electrophoresis*, **9**, 57–59.

Graham, I.A., Leaver, C.J. and Smith, S.M. (1992) Induction of malate synthase gene expression in senescent and detached organs of cucumber. *Plant Cell*, **4**, 349–357.

Graham, I.A., Denby, K.J. and Leaver, C.J. (1994) Carbon catabolite repression regulates glyoxylate cycle gene expression in cucumber. *Plant Cell*, **6**, 761–772.

Gygi, S.P., Rochon, Y., Franza, B.R. and Aebersold, R. (1999) Correlation between protein and mRNA abundance in yeast. *Mol. Cell. Biol.* **19**, 1720–1730.

Hammond-Kosack, K.E. and Rudd, J.J. (2008) Plant resistance signalling hijacked by a necrotrophic fungal pathogen. *Plant Signal. Behav.* **3**, 993–995.

Ipcho, S.V.S., Tan, K.C., Koh, G., Gummer, J., Oliver, R.P., Trengove, R.D. and Solomon, P.S. (2010) The transcription factor StuA regulates central carbon metabolism, mycotoxin production, and effector gene expression in the wheat pathogen *Stagonospora nodorum*. *Eukaryot. Cell*, **9**, 1100–1108.

Janssen, B.J. (1995) A cDNA clone for isocitrate lyase from tomato. *Plant Physiol.* **108**, 1339.

Kale, S.D., Gu, B., Capelluto, D.G.S., Dou, D., Feldman, E., Rumore, A., Arredondo, F.D., Hanlon, R., Fudal, I., Rouxel, T., Lawrence, C.B., Shan, W. and Tyler, B.M. (2010) External lipid PI3P mediates entry of eukaryotic pathogen effectors into plant and animal host cells. *Cell*, **142**, 284–295.

Karpinski, S., Gabrys, H., Mateo, A., Karpinska, B. and Mullineaux, P.M. (2003) Light perception in plant disease defence signalling. *Curr. Opin. Plant Biol.* **6**, 390–396.

Kell, D.B., Brown, M., Davey, H.M., Dunn, W.B., Spasic, I. and Oliver, S.G. (2005) Metabolic footprinting and systems biology: the medium is the message. *Nat. Rev. Microbiol.* **3**, 557–565.

Kim, Y.M., Bouras, N., Kav, N.N.V. and Strelkov, S.E. (2010) Inhibition of photosynthesis and modification of the wheat leaf proteome by Ptr ToxB: a host-specific toxin from the fungal pathogen *Pyrenophora tritici-repentis*. *Proteomics*, **10**, 2911–2926.

Laemmli, U.K. (1970) Cleavage of structural proteins during the assembly of the head of bacteriophage T4. *Nature*, **227**, 680–685.

Levesque-Tremblay, G., Havaux, M. and Ouellet, F. (2009) The chloroplastic lipocalin AtCHL prevents lipid peroxidation and protects Arabidopsis against oxidative stress. *Plant J.* **60**, 691–702.

Liu, J.J., Sturrock, R. and Ekramoddoullah, A.K. (2010) The superfamily of thaumatin-like proteins: its origin, evolution, and expression towards biological function. *Plant Cell Rep.* **29**, 419–436.

Liu, Z., Faris, J.D., Oliver, R.P., Tan, K.C., Solomon, P.S., McDonald, M.C., McDonald, B.A., Nunez, A., Lu, S., Rasmussen, J.B. and Friesen, T.L. (2009) SnTox3 acts in effector triggered susceptibility to induce disease on wheat carrying the Snn3 gene. *PLoS Pathog.* **5**, e1000581.

Liu, Z.H., Faris, J.D., Meinhardt, S.W., Ali, S., Rasmussen, J.B. and Friesen, T.L. (2004) Genetic and physical mapping of a gene conditioning sensitivity in wheat to a partially purified host-selective toxin produced by *Stagonospora nodorum*. *Phytopathology*, **94**, 1056–1060.

Lowe, R.G.T., Lord, M., Rybak, K., Trengove, R.D., Oliver, R.P. and Solomon, P.S. (2009) Trehalose biosynthesis is involved in sporulation of *Stagonospora nodorum*. *Fungal Genet. Biol.* **46**, 381–389.

Manning, V.A., Andrie, R.M., Trippe, A.F. and Ciuffetti, L.M. (2004) Ptr ToxA requires multiple motifs for complete activity. *Mol. Plant-Microbe. Interact,* **17**, 491–501.

Manning, V.A. and Ciuffetti, L.M. (2005) Localization of Ptr ToxA produced by *Pyrenophora tritici-repentis* reveals protein import into wheat mesophyll cells. *Plant Cell*, **17**, 3203–3212.

Manning, V.A., Hardison, L.K. and Ciuffetti, L.M. (2007) Ptr ToxA interacts with a chloroplast-localized protein. *Mol. Plant–Microbe Interact.* **20**, 168–177.

Manning, V.A., Hamilton, S.M., Karplus, P.A. and Ciuffetti, L.M. (2008) The Arg–Gly–Asp-containing, solvent-exposed loop of Ptr ToxA is required for internalization. *Mol. Plant–Microbe Interact.* **21**, 315–325.

Manning, V.A., Chu, A.L., Steeves, J.E., Wolpert, T.J. and Ciuffetti, L.M. (2009) A host-selective toxin of *Pyrenophora tritici-repentis*, Ptr ToxA, induces photosystem changes and reactive oxygen species accumulation in sensitive wheat. *Mol. Plant–Microbe Interact.* **22**, 665–676.

Manning, V.A., Chu, A.L., Scofield, S.R. and Ciuffetti, L.M. (2010) Intracellular expression of a host-selective toxin, ToxA, in diverse plants phenocopies silencing of a ToxA-interacting protein, ToxABP1. *New Phytol.* **187**, 1034–1047.

McLaughlin, J.C. and Smith, S.M. (1994) Metabolic regulation of glyoxylate-cycle enzyme synthesis in detached cucumber cotyledons and protoplasts. *Planta*, **195**, 22–28.

Montillet, J.-L., Chamnongpol, S., Rusterucci, C., Dat, J., van de Cotte, B., Agnel, J.-P., Battesti, C., Inze, D., Van Breusegem, F. and Triantaphylides, C. (2005) Fatty acid hydroperoxides and H_2O_2 in the execution of hypersensitive cell death in tobacco leaves. *Plant Physiol.* **138**, 1516–1526.

Mur, L.A.J., Kenton, P., Lloyd, A.J., Ougham, H. and Prats, E. (2008) The hypersensitive response; the centenary is upon us but how much do we know? *J. Exp. Bot.* **59**, 501–520.

Nieri, B., Ciurli, A., Pistelli, L., Smith, S.M., Alpi, A. and De Bellis, L. (1997) Glyoxylate cycle enzymes in seedlings and in mature plants of tomato (*Lycopersicon esculentum* Mill.). *Plant Sci.* **129**, 39–47.

O'Farrell, P.H. (1975) High resolution two-dimensional electrophoresis of proteins. *J. Biol. Chem.* **250**, 4007–4021.

Oliver, R.P. and Solomon, P.S. (2004) Does the oxidative stress used by plants for defence provide a source of nutrients for pathogenic fungi? *Trends Plant Sci.* **9**, 472–473.

Oliver, R.P., Rybak, K., Solomon, P.S. and Ferguson-Hunt, M. (2009) Prevalence of ToxA-sensitive alleles of the wheat gene Tsn1 in Australian and Chinese wheat cultivars. *Crop and Pasture Science,* **60**, 348–352.

Oliver, R.P. and Solomon, P.S. (2010) New developments in pathogenicity and virulence of necrotrophs. *Curr. Opin. Plant Biol.* **13**, 415–419.

Pandelova, I., Betts, M.F., Manning, V.A., Wilhelm, L.J., Mockler, T.C. and Ciuffetti, L.M. (2009) Analysis of transcriptome changes induced by Ptr ToxA in wheat provides insights into the mechanisms of plant susceptibility. *Mol. Plant*, **2**, 1067–1083.

Parry, M.A.J., Reynolds, M., Salvucci, M.E., Raines, C., Andralojc, P.J., Zhu, X.-G., Price, G.D., Condon, A.G. and Furbank, R.T. (2011) Raising yield potential of wheat. II. Increasing photosynthetic capacity and efficiency. *J. Exp. Bot.* **62**, 453–467.

Paul, M.J. and Pellny, T.K. (2003) Carbon metabolite feedback regulation of leaf photosynthesis and development. *J. Exp. Bot.* **54**, 539–547.

Pistelli, L., De Bellis, L. and Alpi, A. (1991) Peroxisomal enzyme activities in attached senescing leaves. *Planta*, **184**, 151–153.

Rabilloud, T. and Charmont, S. (2000) Detection of proteins on two-dimensional electrophoresis gels. In: *Proteome Research: Two-Dimensional Gel Electrophoresis and Identification Methods* (Rabilloud, T., ed.), pp. 107–125. Berlin, New York: Springer.

Reiner, A., Yekutieli, D. and Benjamini, Y. (2003) Identifying differentially expressed genes using false discovery rate controlling procedures. *Bioinformatics*, **19**, 368–375.

Rudd, J.J., Keon, J. and Hammond-Kosack, K.E. (2008) The wheat mitogen-activated protein kinases TaMPK3 and TaMPK6 are differentially regulated at multiple levels during compatible disease interactions with *Mycosphaerella graminicola*. *Plant Physiol.* **147**, 802–815.

Samuel, M.A., Hall, H., Krzymowska, M., Drzewiecka, K., Hennig, J. and Ellis, B.E. (2005) SIPK signaling controls multiple components of harpin-induced cell death in tobacco. *Plant J.* **42**, 406–416.

Sarma, G.N., Manning, V.A., Ciuffetti, L.M. and Karplus, P.A. (2005) Structure of Ptr ToxA: an RGD-containing host-selective toxin from *Pyrenophora tritici-repentis*. *Plant Cell*, **17**, 3190–3202.

Schauer, N., Steinhauser, D., Strelkov, S., Schomburg, D., Allison, G., Moritz, T., Lundgren, K., Roessner-Tunali, U., Forbes, M.G., Willmitzer, L., Fernie, A.R. and Kopka, J. (2005) GC-MS libraries for the rapid identification of metabolites in complex biological samples. *FEBS Lett.* **579**, 1332–1337.

Scheideler, M., Schlaich, N.L., Fellenberg, K., Beissbarth, T., Hauser, N.C., Vingron, M., Slusarenko, A.J. and Hoheisel J.D. (2002) Monitoring the switch from housekeeping to pathogen defense metabolism in *Arabidopsis thaliana* using cDNA arrays. *J. Biol. Chem.* **277**, 10 555–10 561.

Schottler, M.A., Kirchhoff, H. and Weis, E. (2004) The role of plastocyanin in the adjustment of the photosynthetic electron transport to the carbon metabolism in tobacco. *Plant Physiol.* **136**, 4265–4274.

Shetty, N.P., Jensen, J.D., Knudsen, A., Finnie, C., Geshi, N., Blennow, A., Collinge, D.B. and Jørgensen, H.J.L. (2009) Effects of beta-1,3-glucan from *Septoria tritici* on structural defence responses in wheat. *J. Exp. Bot.* **60**, 4287–4300.

Solomon, P.S. and Oliver, R.P. (2002) Evidence that γ-aminobutyric acid is a major nitrogen source during *Cladosporium fulvum* infection of tomato. *Planta*, **214**, 414–420.

Solomon, P.S., Rybak, K., Trengove, R.D. and Oliver, R.P. (2006) Investigating the role of calcium/calmodulin-dependent protein kinases in *Stagonospora nodorum*. *Mol. Microbiol.* **62**, 367–381.

Sommer, F., Hippler, M., Biehler, K., Fischer, N. and Rochaix, J.D. (2003) Comparative analysis of photosensitivity in photosystem I donor and acceptor side mutants of *Chlamydomonas reinhardtii*. *Plant Cell Environ.* **26**, 1881–1892.

Strelkov, S.E. and Lamari, L. (2003) Host–parasite interactions in tan spot [*Pyrenophara tritici-repentis*] of wheat. *Can. J. Plant Pathol.* **25**, 339–349.

Tai, Y.-S., Bragg, J. and Meinhardt, S. (2007) Functional characterization of ToxA and molecular identification of its intracellular targeting protein in wheat. *Am. J. Plant Physiol.* **2**, 76–89.

Tomas, A., Feng, G.H., Reeck, G.R., Bockus, W.W. and Leach, J.E. (1990) Purification of a cultivar-specific toxin from *Pyrenophora tritici-repentis*, causal agent of tan spot of wheat. *Mol. Plant-Microbe. Interact.* **3**, 221–224.

Torres, M.A. (2010) ROS in biotic interactions. *Physiol. Plant.* **138**, 414–429.

Van Loon, L.C., Rep, M. and Pieterse, C.M.J. (2006) Significance of inducible defense-related proteins in infected plants. *Annu. Rev. Phytopathol.* **44**, 135–162.

Wijekoon, C.P., Goodwin, P.H. and Hsiang, T. (2008) Quantifying fungal infection of plant leaves by digital image analysis using Scion Image software. *J. Microbiol. Methods*, **74**, 94–101.

SUPPORTING INFORMATION

Additional Supporting Information may be found in the online version of this article:

Table S1 Features of the experimental design pertaining to two-dimensional electrophoresis.

Table S2 Observed p*I* and molecular weight (MW), $\log_2$ ratios ($ToxA/H_2O$) and *P* values of the identified proteins.

Table S3 Identities of differentially expressed proteins following matrix-assisted laser desorption ionization time-of-flight tandem mass spectrometry (MALDI TOF/TOF MS/MS) and MASCOT search. C, chloroplastic location; S, secreted protein; –, other location. Spots highlighted in grey contain more than one protein (i.e. cross-contaminations).

Table S4 MASCOT results.

Please note: Wiley-Blackwell are not responsible for the content or functionality of any supporting materials supplied by the authors. Any queries (other than missing material) should be directed to the corresponding author for the article.